



HAL
open science

A proline-rich motif on VGLUT1 reduces synaptic vesicle super-pool and spontaneous release frequency

Xiao Min Zhang, Urielle François, Katlin Silm, Maria Florencia Angelo, Maria Victoria Fernandez-Busch, Mona Maged, Christelle Martin, Veronique Bernard, Fabrice Cordelières, Melissa Deshors, et al.

► To cite this version:

Xiao Min Zhang, Urielle François, Katlin Silm, Maria Florencia Angelo, Maria Victoria Fernandez-Busch, et al.. A proline-rich motif on VGLUT1 reduces synaptic vesicle super-pool and spontaneous release frequency. *eLife*, 2019, 8, pp.e50401. 10.7554/eLife.50401 . hal-02365471

HAL Id: hal-02365471

<https://hal.science/hal-02365471>

Submitted on 15 Nov 2019

HAL is a multi-disciplinary open access archive for the deposit and dissemination of scientific research documents, whether they are published or not. The documents may come from teaching and research institutions in France or abroad, or from public or private research centers.

L'archive ouverte pluridisciplinaire **HAL**, est destinée au dépôt et à la diffusion de documents scientifiques de niveau recherche, publiés ou non, émanant des établissements d'enseignement et de recherche français ou étrangers, des laboratoires publics ou privés.



Distributed under a Creative Commons Attribution 4.0 International License

1 **A proline-rich motif on VGLUT1 reduces synaptic vesicle super-pool and spontaneous**
2 **release frequency**

3
4 Xiao-Min Zhang ^{1,2,3,§}, Urielle François ^{1,2,*}, Katlin Silm ^{4* †}, Maria Florencia Angelo ^{1,2},
5 Maria Victoria Fernández Busch ^{1,2}, Mona Maged ^{1,2}, Christelle Martin ^{1,2}, Véronique Bernard
6 ⁴, Fabrice P. Cordelières ⁵, Melissa Deshors ¹, Stéphanie Pons ⁶, Uwe Maskos ⁶, Alexis-Pierre
7 Bemelmans ^{7,8}, Sonja M. Wojcik ³, Salah El Mestikawy ^{4,9}, Yann Humeau ^{1,2}, Etienne
8 Herzog ^{1,2,#}

9
10 ¹ Interdisciplinary Institute for Neuroscience, Université de Bordeaux, UMR 5297, 33000
11 Bordeaux, France.

12 ² Interdisciplinary Institute for Neuroscience, CNRS UMR 5297, 33000 Bordeaux, France.

13 ³ Department of Molecular Neurobiology, Max Planck Institute of Experimental Medicine, D-
14 37075 Göttingen, Germany.

15 ⁴ Neuroscience Paris Seine NPS, INSERM U1130, CNRS UMR8246, Université Pierre et
16 Marie Curie UM119, 75252 Paris cedex 05, France.

17 ⁵ Bordeaux Imaging Center, Université de Bordeaux, CNRS UMS 3420, INSERM US4,
18 33000, Bordeaux, France.

19 ⁶ Institut Pasteur, CNRS UMR 3571, Unité NISC, Paris, France.

20 ⁷ Commissariat à l'Energie Atomique et aux Energies Alternatives (CEA), Direction de la
21 Recherche Fondamentale (DRF), Institut de Biologie François Jacob (IBFJ), Molecular
22 Imaging Research Center (MIRCen), Fontenay-aux-Roses, France.

23 ⁸ Centre National de la Recherche Scientifique (CNRS), Université Paris-Sud, Université
24 Paris-Saclay, UMR 9199, Neurodegenerative Diseases Laboratory, Fontenay-aux-Roses,
25 France.

26 ⁹ Douglas Mental Health University Institute, Department of Psychiatry, McGill University,
27 Montreal, QC, H4H 1R3, Canada.

28 [§] *Present address*: Department of Neurochemistry, Graduate School of Medicine, The
29 University of Tokyo, Tokyo, 1130033, Japan.

30 [†] *Present address*: Department of Neurology and Department of Physiology, University of
31 California, San Francisco, San Francisco, CA 94143, USA.

32
33 * These authors contributed equally to the work

34
35 # Corresponding and lead contact author: Etienne Herzog; etienne.herzog@u-bordeaux.fr

36
37
38 **Keywords:** proline-rich domain; synaptic vesicle; synaptic vesicle super-pool; vesicular
39 glutamate transporter; liquid phase separation; EndophilinA1; quantal neurotransmitter
40 release; fluorescence live cell microscopy; synaptic vesicle cycle.

42 **ABSTRACT**

43 Glutamate secretion at excitatory synapses is tightly regulated to allow for the precise tuning
44 of synaptic strength. Vesicular Glutamate Transporters (VGLUT) accumulate glutamate into
45 synaptic vesicles (SV) and thereby regulate quantal size. Further, the number of release sites
46 and the release probability of SVs maybe regulated by the organization of active zone proteins
47 and SV clusters. In the present work, we uncover a mechanism mediating an increased SV
48 clustering through the interaction of VGLUT1 second proline-rich domain, endophilinA1 and
49 intersectin1. This strengthening of SV clusters results in a combined reduction of axonal SV
50 super-pool size and miniature excitatory events frequency. Our findings support a model in
51 which clustered vesicles are held together through multiple weak interactions between Src
52 homology 3 and proline-rich domains of synaptic proteins. In mammals, VGLUT1 gained a
53 proline-rich sequence that recruits endophilinA1 and turns the transporter into a regulator of
54 SV organization and spontaneous release.

55

56 **INTRODUCTION**

57 Synaptic vesicles (SVs) engage in multiple protein interactions at the presynaptic active zone
58 (1) and fuse with the presynaptic plasma membrane upon calcium influx, to release their
59 neurotransmitter content (2). Within axon terminals, SVs are segregated from other organelles
60 and grouped in a cluster behind the active zone (3). In adult neurons, SV supply at synapses
61 depends not only on *de novo* vesicle biogenesis, but also on the exchange of mobile SVs
62 between *en passant* boutons along the axon. This exchange pool has been named “SV super-
63 pool” (4-8) and is probably a feature of both glutamatergic and GABAergic axons (9). While
64 the last steps in the regulation of SV release have been studied intensively in different models,
65 the relationship between super-pool SVs, clustered SVs, and the fine-tuning of release at
66 terminals is much less well understood. However, synapsins, a family of SV associated

67 phospho-proteins, play a central role in the regulation of SV clustering and mobility (10,11).
68 A growing body of evidence furthermore suggests that SV cluster formation may result from
69 a liquid phase separation from other cytoplasmic elements (12,13). Phase separation may be
70 induced by the loose interaction of multiple proline-rich (or Poly-Proline; PRD) domains with
71 multiple SH3 (Src Homology 3) domain proteins (14). Indeed, PRD/SH3 interactions are
72 numerous among the actors of SV trafficking such as synapsins and dephosphins (15,16). In
73 addition to these interactions, the actin cytoskeleton may contribute to the scaffolding of SV
74 clusters and SV super-pool motility (5,17-20).

75 Besides SV dynamics and release competence, SV loading with neurotransmitter is another
76 important parameter for the fine-tuning of neurotransmission. To fulfill this function, each
77 excitatory SV may contain between 4 and 14 molecules of Vesicular Glutamate Transporters
78 (21,22). Three isoforms of VGLUTs have been identified, and named VGLUT1-3 (23-28).
79 They share a nearly identical glutamate transport mechanism (29-31) but have distinct
80 expression patterns (32). VGLUT1 is predominantly expressed in pathways of the olfactory
81 bulb, neo-cortex, hippocampus and cerebellum and is associated with low release probability,
82 while VGLUT2 is strongly expressed in sub-cortical pathways of the thalamus and brainstem,
83 and is preferentially associated with high release probability projections (33,34). This
84 observation raised questions regarding a potential role of the VGLUT transporters in tuning
85 SV release probability.

86 Hence, soon after their initial characterization, VGLUT1 and -2 were suspected to bear
87 additional functional features that influence neurotransmitter release beyond quantal size (34-
88 37). We discovered that mammalian VGLUT1, but not -2 or -3, interacts with the SH3
89 domain of endophilinA1 via a proline-rich sequence (38-40). The VGLUT1/EndophilinA1
90 interaction reduces SV release probability (41) and increases the speed of endocytosis of
91 several SV proteins upon long trains of stimulation (39,42). Furthermore, VGLUTs bear

92 several di-leucine motifs on their N- and C- terminal sequences, which are responsible for
93 efficient internalization after exocytosis (39,42-44). The functional relevance of these
94 additional properties of VGLUTs is underscored by the 40% reduction in the number of SVs
95 at *Slc17a7* (VGLUT1) knock-out (VGLUT1 KO) hippocampal Schaffer collateral and
96 cerebellar parallel fiber terminals (34,45). Despite this reduction in clustered SV numbers, SV
97 protein expression is not diminished nor displaced to other subcellular compartments (45).
98 Yet, we unexpectedly discovered a significantly larger SV super-pool in the axons of
99 VGLUT1 KO neurons (45). Also, VGLUT1 KO SVs appear pleomorphic under hyperosmotic
100 chemical fixation (45,46), however this latter phenotype is most likely a direct consequence
101 of a major change in the ionic composition of the SV lumen (29-31,47).
102 In the present work, we determined the minimal domain responsible for the influence of
103 VGLUT1 on the axonal super-pool in mammals. To this end, we generated mutants that
104 disconnect the transport function of VGLUT1 from its trafficking function. We observed that
105 VGLUT1 reduces SV super-pool size as well as the frequency of miniature Excitatory Post-
106 Synaptic Currents (mEPSC) exclusively through the interaction of its PRD2 motif with
107 EndophilinA1. These effects were further mediated by the non-canonical interaction of the
108 VGLUT1/EndophilinA1 complex with the SH3B domain of the presynaptic scaffold protein
109 intersectin1 (15). Taken together, our data support the idea that VGLUT1 fine-tunes SV
110 release by strengthening the liquid phase-separation between clustered and super-pool SVs.

111

112 **RESULTS**

113 **A specific and dose dependent reduction of super-pool size by VGLUT1**

114 We first compared SV exchange between clusters and the axonal super-pool in wild type and
115 VGLUT1 KO littermate primary neuron cultures. To this end, we expressed a tagged
116 synaptobrevin protein (Syb2^{EGFP}) as a reporter (Figure 1A). Through FRAP (fluorescence
117 recovery after photo-bleaching) of boutons we measured higher exchange rates of Syb2^{EGFP}

118 with the axonal compartment, for VGLUT1 KO neurons compared to wild-type neurons
119 (Figure 1B, C, supplementary file 1). A higher exchange rate of VGLUT1 KO SVs with the
120 axonal super-pool is in line with our previous findings (45). We then transduced
121 VGLUT1^{Venus} cDNA (8) to rescue VGLUT1 KO neurons or over-express VGLUT1 in wild
122 type neurons (Figure 1D). FRAP of VGLUT1^{Venus} fluorescence revealed that VGLUT1
123 overexpression further reduces SV exchange with axonal pools compared to the rescue of the
124 knock-out to endogenous levels (Figure 1E). Finally, VGLUT2^{Venus} expression didn't reduce
125 the VGLUT1 KO larger super-pool phenotype (Figure1-figure supplement 1, supplementary
126 file 1). Therefore, VGLUT1 expression in neurons reduces the size of the SV super-pool in a
127 dose dependent manner.

128 **Structure analysis of VGLUT1**

129 To uncover the molecular mechanism by which VGLUT1 regulates SV super-pool size, we
130 generated a series of mutants spanning the sequence of the transporter (Figure 2A and Table
131 1). VGLUT1 contains 12 trans-membrane domains with both termini on the cytoplasmic side
132 and N-glycosylation on the first luminal loop (56). As vesicular glutamate transport strongly
133 impacts SV tonicity, we first aimed at determining whether the SV loading state impacts SV
134 mobility between SV clusters and the axonal super-pool. A triple point mutant R80Q, R176K,
135 R314Q was generated to produce a glutamate transport deficient transporter as previously
136 reported for VGLUT2 (46,56,sVGLUT1 for silent VGLUT1; Figure 2A blue residues; 57).
137 We then focused our efforts on several conserved patterns at the VGLUT1 C-terminus. Indeed,
138 mammalian VGLUT1 displays a unique double proline-rich (PRD1 530-540; PRD2 550-556)
139 pattern conserved in all mammals and absent in VGLUT2 and -3 or in invertebrate orthologs
140 of VGLUT1 (38). We thus generated deletions and point mutations to test the function of the
141 PRD motifs (Figure 2A and Table 1). A conserved 540SYGAT sequence between PRD1 and
142 PRD2 is present in all VGLUT isoforms including invertebrates (38). In addition to the

143 deletion mutants, we also generated S540 and T544 to alanine mutations (Figure 2A and
144 Table 1). We furthermore tested the full deletion of the C-terminus and point mutations in a
145 putative PDZ-type3 binding domain (DQL514; PDZ: Post-synaptic density
146 protein/Drosophila disc large tumor suppressor/Zonula occludens-1; see Figure 2A and Table
147 1).

148 All mutants were tagged using our successful c-terminal strategy (8) and the expression level
149 after transduction was monitored to match the endogenous levels of VGLUT1 using
150 immunoblot (not shown). During FRAP and time-lapse experiments, the first frame of each
151 sequence was used to further check the expression level of each mutant compared to the wild-
152 type control (see examples in Figure 2B and quantification in Figure 2C, D). None of the
153 mutants displayed a significant qualitative or quantitative difference in expression compared
154 to wild-type controls.

155 **Vesicular glutamate uptake function does not influence SV super-pool size.**

156 VGLUT1 KO neurons display hypotonic SVs due to the loss of glutamate transport function
157 (44). To monitor a potential effect of SV lumen tonicity on SV mobility, we transduced
158 VGLUT1^{mCherry} or the triple mutation sVGLUT1^{mCherry} together with Syb2^{EGFP} in VGLUT1
159 KO neurons (Figure 3A) and probed SV turn over at synapses using Syb2^{EGFP} FRAP. While
160 we had a very high percentage of co-transduced neurons, we could find fibers with no
161 VGLUT1^{mCherry} signal and used these as a negative control. Both rescue conditions lowered
162 the exchange of SVs compared to VGLUT1 KO synapses of the same cultures significantly
163 and to the same degree (Figure 3B, supplementary file 1). In patch clamp experiments, a
164 remaining spontaneous activity was found in the knock-out cultures that can be attributed to a
165 minor but significant expression of VGLUT2 in hippocampal neurons (35,58,59). To
166 minimize this contribution we monitored VGLUT2 levels in the culture at several ages and
167 established that the lower plateau is reached between DIV17 and DIV22 when we performed

168 our imaging and patch clamp experiments (see Figure 3-figure supplement 1). As anticipated,
169 sVGLUT1 was unable to rescue the mEPSC amplitude to the same level as the wild type
170 control (Figure 3C, D). The deficiency in the rescue of glutamate transport by sVGLUT1 is
171 also apparent in the frequency of mEPSC events, as empty SVs also cycle (35,60). No impact
172 of sVGLUT1 was seen on mIPSC features (Figure 3- figure supplement 2, supplementary file
173 1). Hence, the triple mutation sVGLUT1 failed to rescue SV loading with glutamate, but
174 reduced SV super-pool size to the same extent as the wild-type control.

175 **VGLUT1 PRD2 domain reduces SV super-pool size and the frequency of miniature**
176 **EPSCs.**

177 We then tested a series of VGLUT1^{venus} mutations spanning the C-terminal cytoplasmic tail of
178 the transporter to rescue the VGLUT1 KO large SV super-pool phenotype (see Figure 2 and
179 Table 1). In the FRAP paradigm, only the mutations disrupting the PRD2 sequence were not
180 able to reduce SV exchange down to WT levels (Figure 4A, B). A point mutation in PRD2
181 (P554A) that blocks the interaction with endophilin is sufficient to increase both the plateau
182 of recovery and the rate of exchange of SVs (shorter slow half-life for P554A, Figure 4A,
183 supplementary file 1). Similar shifts were observed upon deletion of PRD2 (not shown). To
184 further measure SV super-pool size, we performed time-lapse imaging at high sampling rates
185 (5 images per seconds) and tracked VGLUT1^{venus} axonal transport between synaptic boutons
186 (Figure 4C-E). This assay confirmed a significantly larger mobile axonal super-pool of SVs
187 for VGLUT1^{P554A-venus} but not for VGLUT1^{S540A-venus} compared to WT rescue (Figure 4D).
188 Yet, no difference in axonal transport speed could be measured between the 3 constructs
189 (Figure 4E). We also investigated whether PRD2 function could be regulated by
190 phosphorylation of the conserved 540-SYGAT sequence. We thus implemented the PhosTag
191 assay that specifically shifts the electrophoretic mobility of phospho-proteins (55).
192 VGLUT1^{venus} constructs displayed an additional slow band in PhosTag gel migration, except

193 when samples were digested with alkaline phosphatase (Figure 4-figure supplement 1C). All
194 mutants including Δ C-term displayed this second slower band. Thus, VGLUT1 appears to be
195 phosphorylated, but not at the C-terminal tail, and the function of the extremely conserved
196 540-SYGAT sequence therefore remains unclear.

197 In patch-clamp experiments, we tested the effect of VGLUT1^{P554A-venus} rescue on miniature
198 events, compared to WT and empty vector controls (sham; Figure 4F). VGLUT1^{P554A} rescued
199 miniature EPSC amplitudes to a similar level as the wild type transporter (Figure 4G).
200 Interestingly, VGLUT1^{P554A} increased the frequency of miniature events significantly more
201 than the WT rescue (Figure 4H). In contrast to this, mIPSC frequencies were similar in all
202 three conditions (Figure 4I and Figure 4-figure supplement 2, supplementary file 1). As
203 intended in our rescue strategy, VENUS fluorescence intensity at boutons was not
204 significantly different between groups tested by electrophysiology (Figure 4J). Therefore, the
205 PRD2 sequence of mammalian VGLUT1 is sufficient to reduce SV super-pool size and
206 mEPSC frequency.

207 **Intersectin1 interaction with endophilin A1 mediates the reduction of the SV super-pool**
208 **promoted by VGLUT1 expression.**

209 Finally, we performed competition experiments with 3 SH3 domains to investigate the
210 VGLUT1^{PRD2} dependent pathway mediating SV super pool reduction (see Table 1 and Figure
211 5A). SH3 domains fused to the cyan fluorescent protein mCERULEAN3 (50) were
212 overexpressed under control of the human synapsin promoter in neuron cultures from
213 VGLUT1^{venus} mice (Figure 5B). Single boutons from fibers coexpressing mCERULEAN3
214 and VENUS were selected for FRAP experiments. An empty mCerulean3 sham construct was
215 used as negative control and had a VGLUT1^{venus} FRAP curve similar to our previous
216 measurements (Figure 5B, C). The SH3 domain of EndophilinA1 was used to displace
217 endogenous full-length EndophilinA1 to test the contribution of the membrane binding Bin1,

218 Amphiphysin, RVs (BAR) domain. The FRAP curve in this experiment matched the sham
219 control recovery (Figure 5B, C). The SH3 domain of EndophilinA1 mutated at E329K and
220 S336K was over-expressed to displace endogenous EndophilinA1 and block the interaction
221 with the SH3B domain of intersectin1 (61). Endo-SH3^{E329K,S336K} shifted the FRAP recovery to
222 a significantly higher plateau, creating a phenocopy of the VGLUT1^{P554A} and VGLUT1 KO
223 mutants (Figure 5B, C, supplementary file 1). Similarly, the SH3B domain of intersectin1 was
224 over-expressed to displace endogenous intersectin1 from EndophilinA1. ITSN1-SH3B also
225 shifted the FRAP recovery to a higher plateau. Hence, full length intersectin1 may be required
226 for the VGLUT1 mediated reduction of SV super pool (Figure 5B, C). Taken together, these
227 competition experiments reveal the involvement of EndophilinA1 and intersectin1 in a
228 complex with VGLUT1 in the negative regulation of SV super pool size in mammals.

229

230 **DISCUSSION**

231 In the present study we could observe that VGLUT1 PRD2 motif is a negative regulator of
232 SV mobility and mEPSC frequency. Our data support that SV super-pool reduction is
233 mediated by an interaction of endophilinA1 with both VGLUT1 PRD2 and intersectin1 SH3B
234 domains.

235 **Molecular dissection of VGLUT1 functions**

236 Previous works had shown that several dileucine-like motifs are involved in VGLUT1
237 endocytosis (39,42,43) and that the PRD2 of VGLUT1 regulates endocytosis during long
238 trains of stimulation (39). The present data provide the first molecular separation of glutamate
239 transport and SV trafficking functions of VGLUT1. The sVGLUT1 mutant allowed us to test
240 the function of the VGLUT1 backbone structure without potential interference brought by the
241 complex flow of ions occurring through glutamate loading (29-31,57,62). sVGLUT1 revealed
242 that glutamate transport is not related to the negative regulation of SV super-pool size. Instead,

243 our detailed structure-function analysis of VGLUT1 C-terminus showed that the PRD2 motif
244 is necessary and sufficient to inhibit SV exchange between boutons and the axonal super-pool.
245 We further tested a conserved putative type 3 PDZ binding motif (DQL514) and the PRD1
246 pattern but found no significant effect on SV super-pool size. Though we brought evidence
247 for VGLUT1 phosphorylation, putative phosphorylation is not at the C-terminus. It thus
248 remains to be seen whether additional features of the C-terminus such as 540SYGAT can be
249 shown to regulate VGLUT1 tuning of SV mobility.

250 Hence, distinctively from the dileucine based endocytosis of VGLUTs, the C-terminal
251 proline-rich domain PRD2 supports the negative regulation of SV mobility and mEPSC
252 frequency in mammals. SV mobility inhibition is operated independently of glutamate
253 loading processed by the core trans-membrane domains. The structure-function relationship
254 of other conserved sequences remain to be established.

255 **Mammalian VGLUT1 is a molecular player of SV clustering at synapses**

256 Synaptic vesicles are segregated from other organelles in the nerve terminal, and grouped in a
257 cluster (3). It has been proposed that SVs are recruited to the cluster by synapsins to an actin
258 based cytoskeleton (63). Yet, several lines of evidence suggest a different mechanism
259 involving the low affinity binding of many partners forming a liquid phase separation to the
260 rest of the cytosol (12,16,18). Indeed, endophilinA1, intersectin, amphiphysin are abundant
261 within the vesicle cluster (Figure 5-figure supplement 1 and, 16,64) while the binding of SH3
262 domains to proline-rich motifs has been shown to generate liquid phase separations in a
263 synthetic assay (14). Further, synapsins were recently shown to induce liquid phase separation
264 with lipid vesicles (13). Hence, the best model to date infers the liquid phase separation of
265 SVs in a dynamic array of labile interactions between synapsins, dephosphins (endophilins,
266 amphiphysins, EPS15, synaptojanins...) and intersectins.

267 Previously, a slower re-acidification of PRD2 deleted VGLUT1-phluorin probes during long
268 trains of stimulation suggested that the recruitment of endophilinA1 increases the endocytosis
269 efficiency of VGLUT1 SVs (39). However, recent reports indicate that endophilinA1
270 interaction with intersectin1 favors clathrin uncoating (61,65), whereas the clathrin coat was
271 shown to inhibit SV acidification (66). Therefore, the recruitment of endophilinA1 and
272 intersectin1 at SVs may speed up clathrin uncoating and SV acidification. This advocates for
273 new experiments designed to discriminate between an impact of VGLUT1 PRD2 on SV
274 endocytosis versus SV uncoating, consecutive acidification kinetics and clustering. More
275 recently, intersectin1 (ITSN1) SH3B was shown to interact with the SH3 domain of
276 endophilinA1 while preserving the interaction of endophilinA1 with its PRD targets on
277 Dynamin and VGLUT1 (61). Furthermore, intersectin1 may as well interact directly with
278 VGLUT1 through the SH3A domain(67,68). Our present data provide evidence for a
279 reduction of the SV super-pool size to the benefit of the SV clusters mediated by a tripartite
280 complex between VGLUT1 PRD2, endophilinA1 and intersectin1 (VGLUT1/EndoA1/ITSN1,
281 Figure 5). The increase in SV exchange rate when PRD2 is mutated strongly suggests a
282 reduced strength in the interactions scavenging SVs in the cluster (7,8). Yet further
283 investigations using single particle tracking methods will be necessary to address whether
284 VGLUT1 PRD2 reduces SV mobility within synaptic clusters as well (20). Our data also fit
285 well with recent reports of intersectin1 function in the re-clustering of newly endocytosed
286 SVs, and on the nano-scale organization of synapsins at terminals (69,70). Downstream of
287 VGLUT1/EndoA1/ITSN1, the SV super-pool reduction may be driven by interactions of
288 intersectin1 with synapsins (13,70) and/or through remodeling of the actin cytoskeleton
289 surrounding the cluster (71). Yet further analysis will be required to discriminate between
290 these pathways and evaluate a possible regulation by phosphorylation/dephosphorylation
291 cycles.

292 Mammalian VGLUT1 acts as a dual regulator of glutamate release

293 Vesicular glutamate transporters are necessary and sufficient to generate a glutamatergic
294 phenotype in neurons by loading secretory organelles with glutamate (23). Quantal size
295 modulation has been reported upon changes in the level of VGLUT expression (35,36,72) and
296 is reproduced in our present work (Figure 3 and 4). Furthermore, EndophilinA1 binding to the
297 VGLUT1 PRD2 sequence was shown to reduce SV release probability (41). Our dataset now
298 supports the role of VGLUT1/EndoA1/ITSN1 in the reduction of mEPSC frequency and SV
299 exchange between clusters and super-pool (Figure 4 and 5). A discrepancy may arise from the
300 fact that Weston et al. did not see an effect of VGLUT1 Δ PRD2 on mEPSC frequency but
301 only on SV release probability. However, this may be explained by two differences in our
302 recording conditions. First, the autaptic culture system from Weston et al. prevents the
303 formation of a network. Autapses are powerful tools to dissect evoked activity, but mEPSCs
304 in autaptic conditions arise from a single cell (the recorded cell), while in continental cultures
305 they are generated by multiple cells targeting the recorded neuron. Additionally, continental
306 cultures build a network that generates activity, which most likely leads to different set-points
307 of SV super-pool sizes and homeostatic plasticity compared to autaptic micro-islands (73).
308 Second, Weston and colleagues worked before 14 days in culture, whereas we worked after
309 17 days in culture when VGLUT2 expression reached a lower plateau and may generate less
310 background mEPSC activity (Figure 3- figure supplement 1; 35,59).

311 The molecular mechanism of SV super-pool reduction that we uncovered requires the
312 EndoA1 SH3 domain, but not the BAR domain (Figure 5). Previously, Weston et al. showed
313 that endophilinA1 promotes SV release probability through dimerization and BAR domain
314 mediated membrane binding (41). Our current results complement this model by adding a
315 pathway through which VGLUT1/EndoA1 recruit intersectin1 to promote SV clustering and
316 mEPSC frequency reduction in a BAR domain independent fashion. Hence, free

317 EndophilinA1 may actively promote SV exocytosis through membrane binding mechanisms
 318 while VGLUT1-bound EndophilinA1 may actively reduce SV mobility and exocytosis
 319 through an intersectin1 dependent pathway.

320 Beyond setting the quantal size, VGLUT1 influences glutamate release parameters most
 321 likely by changing the strength of SVs phase separation in clusters. It remains to establish
 322 how neurons take advantage of this feature to locally modulate the parameters of quantal
 323 release at selected synapses (7,8,74). In this line, neuromodulation has been very recently
 324 proposed to tune SV pools in the axon through GPCR signaling and synapsin phosphorylation
 325 (75).

326 MATERIALS & METHODS

| Key Resources Table | | | | |
|--|---|---------------------|---|--|
| Reagent type (species) or resource | Designation | Source or reference | Identifiers | Additional information |
| strain, strain background (<i>Mus musculus</i>) | <i>Slc17a7</i> ^{-/-} (VGLUT1 KO) mice | PMID: 15103023 | available upon request to Dr Sonja M. Wojcik wojcik@em.mpg.de | |
| strain, strain background (<i>Mus musculus</i>) | <i>Slc17a7</i> ^{+/v} (VGLUT1venus KI) mice | PMID: 22031900 | available upon request to corresponding author | |
| transfected construct (<i>Homo sapiens</i>) | F(syn)W-RBN::Synaptobrevin2-EGFP | PMID: 23581566 | available upon request to Dr. Etienne Herzog | Fig1, Fig3 and related results part. Lentiviral vector expressing Syb2EGFP. |
| transfected construct (<i>Rattus norvegicus</i>) | F(syn)W-RBN::VGLUT1-venus | PMID: 23581566 | available upon request to Dr. Etienne Herzog | Fig1, Fig4 and related results part. Lentiviral vector expressing VGLUT1venus. |

| | | | | |
|---|-------------------------------------|------------|--|---|
| transfected construct (<i>Rattus norvegicus</i>) | F(syn)W-RBN::VGLUT2-venus | This paper | available upon request to Dr. Etienne Herzog | Fig1-S1 and related results part. Lentiviral vector expressing VGLUT2venus. |
| transfected construct (<i>Rattus norvegicus</i>) | F(syn)W-RBN::VGLUT1 ΔC-term-venus | This paper | available upon request to Dr. Etienne Herzog | Fig4 and related results part. Lentiviral vector expressing VGLUT1ΔC-term-venus. |
| transfected construct (<i>Rattus norvegicus</i>) | F(syn)W-RBN::VGLUT1 DQL514AQA-venus | This paper | available upon request to Dr. Etienne Herzog | Fig4 and related results part. Lentiviral vector expressing VGLUT1DQL514A QA-venus. |
| transfected construct (<i>Rattus norvegicus</i>) | F(syn)W-RBN::VGLUT1 ΔPRD1+2-venus | This paper | available upon request to Dr. Etienne Herzog | Fig4 and related results part. Lentiviral vector expressing VGLUT1ΔPRD1+2-venus. |
| transfected construct (<i>Rattus norvegicus</i>) | F(syn)W-RBN::VGLUT1 PP534AA-venus | This paper | available upon request to Dr. Etienne Herzog | Fig4 and related results part. Lentiviral vector expressing VGLUT1PP534AA-venus. |
| transfected construct (<i>Rattus norvegicus</i>) | F(syn)W-RBN::VGLUT1 S540A-venus | This paper | available upon request to Dr. Etienne Herzog | Fig4 and related results part. Lentiviral vector expressing VGLUT1S540A-venus. |
| transfected construct (<i>Rattus norvegicus</i>) | F(syn)W-RBN::VGLUT1 T544A-venus | This paper | available upon request to Dr. Etienne Herzog | Fig4 and related results part. Lentiviral vector expressing VGLUT1T544A-venus. |
| transfected construct (<i>Rattus norvegicus</i>) | F(syn)W-RBN::VGLUT1 ΔPRD2-venus | This paper | available upon request to Dr. Etienne Herzog | Fig4 and related results part. Lentiviral vector expressing VGLUT1ΔPRD2-venus. |

| | | | | |
|---|--|------------|--|--|
| transfected construct (<i>Rattus norvegicus</i>) | F(syn)W-RBN::VGLUT1 P554A-venus | This paper | available upon request to Dr. Etienne Herzog | Fig4 and related results part. Lentiviral vector expressing VGLUT1P554A-venus. |
| transfected construct (<i>Rattus norvegicus</i>) | AAV9::VGLUT1mCherry-miniSOG | This paper | available upon request to Dr. Etienne Herzog | Fig3 and related results part. Lentiviral vector expressing VGLUT1mCherry-miniSOG. |
| transfected construct (<i>Rattus norvegicus</i>) | AAV9::sVGLUT1mCherry-miniSOG | This paper | available upon request to Dr. Etienne Herzog | Fig3 and related results part. Lentiviral vector expressing sVGLUT1mCherry-miniSOG. |
| transfected construct (<i>Homo sapiens</i>) | AAV9::mCerulean3-EndophilinA1SH3 | This paper | available upon request to Dr. Etienne Herzog | Fig5 and related results part. Lentiviral vector expressing mCerulean3-EndophilinA1SH3. |
| transfected construct (<i>Homo sapiens</i>) | AAV9::mCerulean3-EndophilinA1SH3 ^{E329K, S336K} | This paper | available upon request to Dr. Etienne Herzog | Fig5 and related results part. Lentiviral vector expressing mCerulean3-EndophilinA1SH3 ^{E329K, S336K} . |
| transfected construct (<i>Homo sapiens</i>) | AAV9::mCerulean3-IntersectinSH3B | This paper | available upon request to Dr. Etienne Herzog | Fig5 and related results part. Lentiviral vector expressing mCerulean3-IntersectinSH3B. |
| antibody | GFP, Mouse, monoclonal | Roche | Cat. 11814460001 RRID: AB_390913 | 1:1000 |
| antibody | VIAAT, Guinea pig, polyclonal | SYSY | Cat. 131004 RRID:AB_887873 | 1:1000 |

| | | | | |
|------------------------------------|---|----------------------|--|---|
| antibody | VGLUT2, Guinea pig, polyclonal | Millipore | Cat. AB2251 RRID:AB_1587 626 | 1:2000 |
| antibody | VGLUT1, guinea pig, polyclonal | Merck | Cat. AB5905 RRID:AB_2301 751 | 1:5000 |
| antibody | EndophilinA1, rabbit, polyclonal | PMID: 16606361 | available upon request to Dr. Etienne Herzog | 1:500 |
| peptide, recombinant protein | FastAP Thermosensitiv e Alkaline Phosphatase | Thermo Scientific | Cat. EF0651 | |
| peptide, recombinant protein | Halt™ phosphatase inhibitor cocktail | Thermo Scientific | Cat. 78420 | |
| chemical compound, drug | Phos-tag Acrylamid | Wako | Cat. AAL-107 | |
| software, algorithm | FRAP Analysis Plugin | This paper | | The plugin is available at: https://github.com/abricecordelieres/IJ-Macro_FRAP-MM |
| software, algorithm | KymoToolbox Plugin | PMID: 23374344 | | The plugin is available at: https://github.com/abricecordelieres/IJ-Plugin_KymoToolBox |

327

328 **Animals**329 All *Slc17A7*^{-/-} (VGLUT1 KO) (35) and *Slc17A7*^{+/v} (VGLUT1^{venus} knock-in) (8) and mice

330 were maintained in C57BL/6N background and housed in 12/12 LD with ad libitum feeding.

331 Every effort was made to minimize the number of animals used and their suffering. The

332 experimental design and all procedures were in accordance with the European guide for the

333 care and use of laboratory animals and approved by the ethics committee of Bordeaux
334 Universities (CE50) under the APAFIS n°1692.

335 **Plasmids and viral vectors**

336 From the Lentivector F(syn)W-RBN::VGLUT1^{venus} previously published (45), we engineered
337 a series of point and deletion mutations of VGLUT1^{venus} using conventional site directed
338 mutagenesis protocols (see Table 1). Some experiments were performed using enhanced
339 green fluorescent protein tagged synaptobrevin2 (F(syn)W-RBN::Syb2EGFP; 45). Lentiviral
340 particles were generated by co-transfection of HEK-293T cells with the vector plasmid, a
341 packaging plasmid (CMVD8.9 or CMV-8.74) and an envelope plasmid (CMV-VSVg) using
342 Lipofectamine Plus (Invitrogen, Carlsbad, CA, USA) according to the manufacturer's
343 instructions. 48h after transfection, viral particles were harvested in the supernatant, treated
344 with DNaseI and MgCl₂, passed through a 0.45 µm filter and concentrated by
345 ultracentrifugation ($\omega^2t = 3,2 \cdot 10^{10} \text{ rad}^2/\text{s}$) and suspended in a small volume of PBS. Viral
346 stocks were stored in 10µl aliquots at -80° C before use. Viral titres were estimated by
347 quantification of the p24 capsid protein using the HIV-1 p24 antigen immunoassay
348 (ZeptoMetrix Corporation, Buffalo, NY, USA) according to the manufacturer's instructions.
349 All productions were between 100 and 300ng/µl of p24. Alternatively, recombinant adeno-
350 associated virus vectors (AAV) were engineered with either WT or the transport deficient
351 sVGLUT1 inserts (see Table 1). We tagged these constructs with mCherry-miniSOG (48).
352 Serotype 9 AAV particles were generated by transient transfection of HEK293T cells and
353 viral stocks were tittered by QPCR on the recombinant genome as previously described (49).
354 Both viral vectors control the expression of the inserts through the human synapsin promoter.
355 For competition experiments with endophilinA1 and intersectin1 SH3 domains, we built
356 fusions of the endophilinA1 SH3 domain (aa 290 to aa 352) or the SH3B domain of
357 intersectin1 (aa 903 to 971) with the fluorescent protein mCerulean3 positioned at their N-

358 terminus (50). All three SH3 domains were synthesized and the sequences checked (Eurofins
359 genomics company). These fusions were cloned into the AAV shuttle plasmid.

360 **Hippocampal cell cultures and transgene expression**

361 Hippocampal primary dissociated cultures were prepared from P0 mice. The hippocampi were
362 dissected in ice-cold Leibovitz's L-15 medium (11415064; Gibco), and then incubated in
363 0.05% trypsin-EDTA (25300054, Gibco) for 15 min at 37°C. The tissues were washed with
364 Dulbecco's Modified Eagle's Medium (DMEM, 61965026, Gibco) containing 10% FBS
365 (CVF5VF0001, Eurobio), 1% Penicillin-streptomycin (15140122, Gibco). Cells were
366 mechanically dissociated by pipetting up and down, and plated onto poly-L-lysine (P2636,
367 Sigma) coated coverslips at a density of 20 000 cells/cm². Cells were grown in Neurobasal A
368 medium (12349105, Gibco) containing 2% B27 supplement (17504044, Gibco), 0.5 mM
369 Glutamax (35050038, Gibco), and 0.2% MycoZap plus-PR (VZA2021, Lonza) for 5 days in-
370 vitro (DIV). From DIV 5-6, complete Neurobasal A medium was partially replaced to ½ by
371 BrainPhys medium (51), every two or three days. Imaging of live dissociated neuron cultures
372 was performed at DIV 17-21 in culture medium with Hepes buffer (40 mM). Neurons were
373 transduced at DIV1 or -2 with viral vectors diluted by a factor 1/1000. The viral expression
374 levels were controlled by both western-blot (not shown), and fluorescence intensity to rescue
375 VGLUT1 expression to endogenous VGLUT1 level. The bouton size and fluorescent
376 intensity from the different VGLUT1 mutants were analyzed from the first frames the FRAP
377 sequences. Images were processed by "Find Edges", binary images were created through a
378 threshold setting application to define the boundary of boutons. Area and background
379 subtracted fluorescence intensity were measured. Integrated intensity values were normalized
380 to the value in WT boutons of the same group. The statistical significance of the bouton size
381 and fluorescence intensity between the WT and VGLUT1 mutant rescues were evaluated with
382 unpaired *t*-tests. For competition experiments with endophilinA1 and intersectin1 SH3

383 domains, plasmids were delivered by electroporation at DIV0 before plating (Nucleofector,
384 Lonza).

385 **FRAP imaging**

386 Fluorescence Recovery After Photobleaching (FRAP) experiments were performed to
387 determine the mobility of Syb2 labeled SVs (for silent VGLUT1 mutant rescue experiments)
388 or VGLUT1 labeled SVs (for VGLUT1 C-terminal mutants rescue experiments) at synapses.
389 The mobile fraction of Syb2/VGLUT1 labeled SVs is the proportion of fluorescent material
390 that can be replenished after photo bleaching. FRAP was performed using a spinning-disk
391 confocal head Yokogawa CSU-X1 (Yokogawa Electric Corporation, Tokyo, Japan) mounted
392 on an inverted Leica DMI 6000 microscope (Leica Microsystems, Wetzlar, Germany) and
393 equipped with a sensitive EM-CCD QuantEM camera (Photometrics, Tucson, USA), and a
394 FRAP scanner system (Roper Scientific, Evry, France). Surrounding the setup, a thermal
395 incubator was set to 37°C (Life Imaging Services, Switzerland). Z-stacks of 4.8 μm thickness
396 were obtained with a piezo P721.LLQ (Physik Instrumente, Karlsruhe, Germany) at randomly
397 selected fields from hippocampal cell culture with a 63 \times /1.4 numerical aperture oil-
398 immersion objective. For each stack, five fluorescent boutons, distant from each other, were
399 selected for bleaching. Three passes of the 491 nm laser (40 mW) for Syb2^{EGFP} or two laser
400 passes using the 491 nm laser (30 mW) and the 405 nm laser (10 mW) for VGLUT1^{venus},
401 were applied on the mid-plane of the stack and resulted in an average bleaching of 50% of the
402 initial fluorescence intensity at boutons. The bleaching protocol for Venus/EYFP prevents the
403 spontaneous recovery of fluorescence from a dark reversible photochemical state as
404 previously reported (8,52).

405 Fluorescence recovery was monitored every 30 s during the first 3 min and then every 5 min
406 during the next 70 min. The entire FRAP procedure was controlled by MetaMorph
407 (Molecular Devices, Sunnyvale, USA). Image processing was automated using ImageJ macro

408 commands (53) (available at https://github.com/fabricecordelieres/IJ-Macro_FRAP-MM).

409 Sum projections of the individual stacks, assembly and *x-y* realignment were applied,

410 resulting in 32 bits/pixel sequences. Integrated fluorescence intensities of the five bleached

411 boutons, and the cells in the field, as well as one background area were extracted. The

412 background signal was subtracted, and data were normalized to the average baseline before

413 bleaching (100%) and corrected for photobleaching against the cells. Experiments were

414 discarded if photobleaching exceeded 60% (risk of phototoxicity). Fluorescence intensity of

415 boutons was normalized to 1 before bleaching, and 0 right after bleaching. A double

416 exponential function was used to fit the average of all normalized FRAP traces and the extra

417 sum-of-squares F test was applied to compare the different best fits. Unpaired t-test was

418 applied to analysis of bouton fluorescence intensity between different mutants and the

419 corresponding WT data sets.

420

421 **Live Cell imaging**

422 Time-lapse experiments using the spinning disk confocal microscope were performed to

423 quantify the SVs moving along the inter-synaptic axonal segments. Images were sampled at 5

424 frames/s for 30 seconds with 200 ms exposure time (151 frames in total). Synaptic boutons

425 were saturated in order to allow better visualization of the dimmer fluorescent material

426 moving along the axons. Quantification of the speed of moving clusters was performed with

427 the KymoToolbox plugin in ImageJ (Figure 4; available at

428 https://github.com/fabricecordelieres/IJ-Plugin_KymoToolBox) (54). In each sequence, 8

429 axons segments of 10-15 μm were selected for particle tracking. Furthermore, the traffic at

430 inter-synaptic segments was quantified by drawing line ROIs perpendicularly to the axon, and

431 cumulating the integrated density values in each of the 151 images. Background was

432 subtracted, and all values were divided by the average of 10 lowest values of the sequence to

433 normalize for the differences of fluorescence intensity between different sets of experiments.
434 All normalized values from each line selection were summed to evaluate the total amount of
435 material going through the given cross-section. The statistical significance of the differences
436 in cumulative traffic between the WT and VGLUT1 mutants (S540A and P554A) were
437 evaluated with unpaired *t*-test.

438 **Electrophysiology**

439 Dual whole-cell patch-clamp recordings were performed from DIV17 to DIV21. Patch
440 pipettes (2-4M Ω) were filled with the following intracellular solution (in mM): 125 CsMeSO₃,
441 2 MgCl₂, 1 CaCl₂, 4 Na₂ATP, 10 EGTA, 10 HEPES, 0.4 NaGTP and 5 QX-314-Cl, pH was
442 adjusted to 7.3 with CsOH. Extracellular solution was a standard ACSF containing the
443 following components (in mM): 124 NaCl, 1.25 NaH₂PO₄, 1.3 MgCl₂, 2.7 KCL, 26 NaHCO₃,
444 2 CaCl₂, 18.6 Glucose and 2.25 Ascorbic acid. To record excitatory and inhibitory miniature
445 currents (mEPSC and mIPSC), Tetrodotoxin (TTX) was added at 1 μ M into an aliquot of the
446 standard ACSF (Alomone labs). Cultures were perfused at 35°C with an ACSF perfusion
447 speed of 0.02mL/min and equilibrated with 95% O₂/5% CO₂. Signals were recorded at
448 different membrane potentials under voltage clamp conditions for about 2 min (0mV for
449 inhibitory events and -70mV for excitatory events) using a MultiClamp 700B amplifier
450 (Molecular Devices, Foster City, CA) and Clampfit software. Recording at 0mV in voltage
451 clamp allowed us to confirm the effect of TTX on network activity. The recording of
452 miniature events began 2min after adding TTX and the extinction of synchronized IPSCs.
453 Additional recordings were performed at membrane potentials of -20mV, -40mV, -60mV and
454 -80mV. For drug treatment, CNQX was used at 50 μ M and PTX at 100 μ M and 2minutes after
455 drug addition, the condition was considered as stable.

456 **Electrophysiology Analysis**

457 Analyses were performed using Clampfit (Molecular Device), in which we created one mini-
458 excitatory (-70mV) and one mini-inhibitory (0mV) template from a representative recording.
459 Those templates were used for all recordings and analysis was done blind to the experimental
460 group. We measured the number of mEPSCs at -70mV and mIPSCs at 0mV and their mean
461 amplitude. Cell properties were monitored to get a homogenous set of cells, i.e. we analyzed
462 the seal-test recordings of every cell (see supplementary file 2) and calculated the capacitance
463 from the Tau measured by Clampfit (supplementary file 2). Cells with a leak current over -
464 200pA, and/or a membrane resistance over -100MOhms were excluded from the analysis.
465 Statistical analyses were performed using One-way ANOVA or Kruskal-Wallis test (* for $p <$
466 0.05, ** for $p < 0.01$ and *** for $p < 0.001$).

467 **Antisera**

468 The detection of wild type VGLUT1 was performed with rabbit polyclonal antiserum (8,25)
469 whereas the detection of VGLUT1^{venus} was done with a mouse monoclonal anti-GFP antibody
470 (11814460001, Roche). Anti-VIAAT (131004, SYSY) and Anti-VGLUT2 (AB2251,
471 Millipore) guinea pig polyclonal antisera were used. For electron microscopy we used a
472 guinea pig anti-VGLUT1 polyclonal antiserum (AB5905, Merck) and a rabbit polyclonal
473 antiserum against endophilinA1 (38). Secondary HRP-coupled anti-rabbit, anti-mouse and
474 anti-guinea pig antibodies were used for western blot detection (711-035-152, 715-035-150,
475 706-035-148, respectively, Jackson ImmunoResearch).

476 **Immunocytochemistry**

477 Neuron cultures were washed with cold 1X PBS and fixed with 4% paraformaldehyde in 1X
478 PBS for 5min at room temperature. Immunostainings were performed as previously described
479 (25). Wide-field pictures were acquired using an epifluorescence Nikon Eclipse NIS-element
480 microscope with the 40x objective. The ImageJ software was used to quantify the
481 fluorescence intensity. A mean filter, background subtraction, and threshold were applied to

482 cover the punctate signals and generate a selection mask. The mean density values were
483 extracted. The averages of 5 frames per culture were probed and more than 3 cultures per age
484 were measured.

485 **Immunohistochemistry and electron microscopy**

486 VGLUT1 and EndophilinA1 were simultaneously detected by combination of
487 immunoperoxidase and immunogold methods, respectively, on brain sections at the
488 ultrastructural level.

489 *Animals and tissue preparation* The mice were deeply anesthetized with sodium chloral
490 hydrate and then perfused transcardially with 0.9% NaCl, followed by fixative consisting
491 of 2% paraformaldehyde (PFA) with 0.2% glutaraldehyde in 0.1M phosphate buffer (PB),
492 pH 7.4, at 4°C. The brain was quickly removed and left overnight in 2% PFA at 4°C.
493 Sections from cerebellum and caudate putamen were cut on a vibrating microtome at
494 70mm and collected in PBS (0.01M phosphate, pH 7.4). To enhance the penetration of
495 the immunoreagents in the preembedding procedures, the sections were equilibrated in
496 a cryoprotectant solution (0.05MPB, pH 7.4, containing 25% sucrose and 10% glycerol)
497 and freeze-thawed by freezing in isopentane cooled in liquid nitrogen and thawed in PBS.
498 The sections were then preincubated in 4% normal goat serum (NGS) in PBS.

499 *Double detection of VGLUT1 and EndophilinA1 by combined preembedding*
500 *immunoperoxidase and immunogold methods.* The brain sections were incubated in 4%
501 NGS for 30 min and then in a mixture of VGLUT1 (1:5000) and EndophilinA1 (1:500)
502 antibodies, supplemented with 1% NGS overnight at RT. The sections were then
503 incubated with goat anti-guinea-pig IgGs conjugated to biotin (1:200), washed in PBS
504 and incubated in a mixture of avidin–biotin–peroxidase complex (ABC), (1:100; Vector
505 Laboratories, Burlingame, CA) and goat anti-rabbit IgGs conjugated to gold particles (1.4
506 nm diameter; Nanoprobes, Stony Brook, N Y; 1:100 in PBS/ BSA-C) for 2 hr in PBS/ BSA-

507 C. The sections were then washed in PBS and post-fixed in 1% glutaraldehyde in PBS.
508 After washing (PBS; sodium acetate buffer, 0.1M, pH 7.0), the diameter of the gold
509 immunoparticles was increased using a silver enhancement kit (HQ silver; Nanoprobes)
510 for 5min at RT in the dark. After washing (2xPBS, 1xTB 0.05M, pH 7.6), the
511 immunoreactive sites VGLUT1 were revealed using DAB. The sections were then stored
512 in PB and processed for electronmicroscopy.

513 *Preparation for electron microscopy* The sections were post-fixed in osmium tetroxide
514 (1% in PB, 0.1M,pH7.4) for 10 min at RT. After washing, they were dehydrated in an
515 ascending series of dilutions of ethanol that included 1% uranyl acetate in 70% ethanol.
516 They were then treated with propylene oxide and equilibrated in resin overnight
517 (Durcupan AC M; Fluka, Buchs, Switzerland), mounted on glass slides, and cured at 60°C
518 for 48 hr. The immunoreactive areas identified on thick sections were cut in semithin
519 sections (1-mm-thick), then in ultrathin sections on a Reichert Ultracut S.
520 Ultrathinsections were collected on pioloform-coated single slot copper grids. The
521 sections were stained with lead citrate and examined in a Philips C M10 electron
522 microscope.

523 **Biochemistry**

524 All steps were performed at 4°C or on ice. Brains of wild type adult mice were dissected for
525 the collection of brain regions. The samples were treated with homogenization buffer (0.32 M
526 sucrose, 4 mM HEPES pH 7.4). Cultures expressing the different VGLUT1 mutants were
527 collected on DIV 17 with 1× PBS. Both buffers were supplemented with protease inhibitor
528 cocktail (539134, Millipore) and HaltTM phosphatase Inhibitor Cocktail (78420, Thermo
529 Fisher Scientific). When necessary, protein samples were treated with alkaline phosphatase
530 prior to the biochemical analysis. FastAP Thermosensitive Alkaline Phosphatase (1 unit/μl)
531 and FastAP 10× buffer (EF0654, Thermo Scientific) were added to samples and incubated for

532 1 h at 37°C. Sodium dodecylsulfate polyacrylamide gel electrophoresis (SDS-PAGE) and
533 phosphate affinity SDS-PAGE (55) were conducted according to standard methods. For
534 phosphate affinity SDS-PAGE (Mn²⁺-Phos-tag SDS-PAGE), 25 μM Phostag (AAL-107,
535 Wako) and 0.1 mM MnCl₂ were added to the resolving gel before polymerization. Western
536 blotting was performed according to standard procedures using HRP-coupled secondary
537 antibodies for qualitative detection. Chemi-luminescence signals were visualized with
538 ChemiDoc MP System (Bio-Rad) using SuperSignalTM West Dura Extended Duration
539 Substrate (34075, Thermo Scientific).

540

541 SOURCE DATA FILES

542 Source data used to build figures are available in the following separate supplementary files:
543 Figure 1-source data 1.xlsx ; Figure 1-source data 2.xlsx ; Figure 1-figure supplement1 source
544 data 1.xlsx ; Figure 2-source data 1.xlsx ; Figure 3-source data 1.xlsx ; Figure 3-source data
545 2.xlsx ; Figure 3-figure supplement 1 source data.xlsx ; Figure 4-source data 1.xlsx ; Figure 4-
546 source data 2.xlsx ; Figure 4-source data 3.xlsx ; Figure 4-source data 4.xlsx ; Figure 4-source
547 data 5.xlsx ; Figure 4-source data 6.xlsx ; Figure 4-source data 7.xlsx ; Figure 4-source data
548 8.xlsx ; Figure 4-source data 9.xlsx ; Figure 4-figure supplement 2 source data.xlsx ; Figure 5-
549 source data 1.xlsx

550 ACKNOWLEDGEMENTS

551 Elisa Luquet, Sally Wenger, and Charlène Josephine for excellent technical support. Nils
552 Brose for a strong support throughout the project. Serge Marty and Martin Oheim for fruitful
553 discussions. Christian Rosenmund, Prof Roger Tsien, Prof Mark A Rizzo, for sharing
554 reagents. Several experiments required the use of Bordeaux University/CNRS/INSERM core
555 facilities: Bordeaux Imaging Center (member of France BioImaging supported by the French
556 National Research Agency; ANR-10-INBS-04); Vect'UB viral vector facility; Biochemistry
557 and Biophysics of Proteins core facility; Mouse breeding facility. X.M.Z. was supported by
558 the Erasmus Mundus ENC program and the labex BRAIN extension grant (ANR-10-LABX-
559 43 BRAIN). Funding from the Agence Nationale de la Recherche (ANR-12-JSV4-0005-
560 01 VGLUT-IQ ; ANR-10-LABX-43 BRAIN; ANR-10-IDEX-03-02 PEPS SV-PIT to E.H.
561 and PSYVGLUT 09-MNPS-033 to S.E.M.). K.S. and M.F.A. were supported by the
562 Fondation pour la Recherche Médicale (FDT20120925288 and ING20150532192
563 respectively).

564 CONFLICT OF INTEREST

565 The authors declare no conflict of interest.

566 **REFERENCES**

- 567
- 568 1. Südhof TC, Rizo J. Synaptic vesicle exocytosis. *Cold Spring Harb Perspect Biol.* 2011
569 Dec;3(12).
- 570 2. Lisman JE, Raghavachari S, Tsien RW. The sequence of events that underlie quantal
571 transmission at central glutamatergic synapses. *Nat Rev Neurosci.* 2007 Aug;8(8):597–
572 609.
- 573 3. Gray EG. Axo-somatic and axo-dendritic synapses of the cerebral cortex: an electron
574 microscope study. *J Anat.* 1959 Oct;93:420–33.
- 575 4. Kraszewski K, Daniell L, Mundigl O, De Camilli P. Mobility of synaptic vesicles in
576 nerve endings monitored by recovery from photobleaching of synaptic vesicle-
577 associated fluorescence. *J Neurosci.* 1996 Oct 1;16(19):5905–13.
- 578 5. Darcy KJ, Staras K, Collinson LM, Goda Y. Constitutive sharing of recycling synaptic
579 vesicles between presynaptic boutons. *Nat Neurosci.* 2006 Feb 8;9(3):315–21.
- 580 6. Westphal V, Rizzoli S, Lauterbach M, Kamin D, Jahn R, Hell S. Video-Rate Far-Field
581 Optical Nanoscopy Dissects Synaptic Vesicle Movement. *Science.* 2008 Feb 21.
- 582 7. Staras K, Branco T, Burden JJ, Pozo K, Darcy K, Marra V, et al. A Vesicle Superpool
583 Spans Multiple Presynaptic Terminals in Hippocampal Neurons. *Neuron.* 2010 Jan
584 4;66(1):37–44.
- 585 8. Herzog E, Nadrigny F, Silm K, Biesemann C, Helling I, Bersot T, et al. In vivo
586 imaging of intersynaptic vesicle exchange using VGLUT1 Venus knock-in mice. *J*
587 *Neurosci.* 2011 Oct 26;31(43):15544–59.
- 588 9. Wierenga CJ, Becker N, Bonhoeffer T. GABAergic synapses are formed without the
589 involvement of dendritic protrusions. *Nat Neurosci.* 2008 Aug 24;11(9):1044–52.
- 590 10. Pieribone VA, Shupliakov O, Brodin L, Hilfiker-Rothenfluh S, Czernik AJ, Greengard
591 P. Distinct pools of synaptic vesicles in neurotransmitter release. *Nature.* 1995 Jun
592 8;375(6531):493–7.
- 593 11. Song S-H, Augustine GJ. Synapsin Isoforms and Synaptic Vesicle Trafficking. *Mol*
594 *Cells.* 2015 Nov 30;38(11):936–40.
- 595 12. Milovanovic D, De Camilli P. Synaptic Vesicle Clusters at Synapses: A Distinct
596 Liquid Phase? *Neuron.* 2017 Mar 8;93(5):995–1002.
- 597 13. Milovanovic D, Wu Y, Bian X, De Camilli P. A liquid phase of synapsin and lipid
598 vesicles. *Science.* 2018 Jul 5.
- 599 14. Li P, Banjade S, Cheng H-C, Kim S, Chen B, Guo L, et al. Phase transitions in the
600 assembly of multivalent signalling proteins. *Nature.* 2012 Mar 7;483(7389):336–40.
- 601 15. Slepnev VI, De Camilli P. Accessory factors in clathrin-dependent synaptic vesicle
602 endocytosis. *Nat Rev Neurosci.* 2000 Dec 1;1(3):161–72.

- 603 16. Pechstein A, Shupliakov O. Taking a back seat: synaptic vesicle clustering in
604 presynaptic terminals. *Front SynNeurosci.* 2010;2:143.
- 605 17. Morales M, Colicos MA, Goda Y. Actin-dependent regulation of neurotransmitter
606 release at central synapses. *Neuron.* 2000 Oct 31;27(3):539–50.
- 607 18. Sankaranarayanan S, Atluri PP, Ryan TA. Actin has a molecular scaffolding, not
608 propulsive, role in presynaptic function. *Nat Neurosci.* 2003 Feb;6(2):127–35.
- 609 19. Shupliakov O, Bloom O, Gustafsson JS, Kjaerulff O, Low P, Tomilin N, et al.
610 Impaired recycling of synaptic vesicles after acute perturbation of the presynaptic actin
611 cytoskeleton. *Proc Natl Acad Sci USA.* 2002 Oct 29;99(22):14476–81.
- 612 20. Gramlich MW, Klyachko VA. Actin/Myosin-V- and Activity-Dependent Inter-synaptic
613 Vesicle Exchange in Central Neurons. *Cell Rep.* 2017 Feb 28;18(9):2096–104.
- 614 21. Takamori S, Holt M, Stenius K, Lemke EA, Grønberg M, Riedel D, et al. Molecular
615 anatomy of a trafficking organelle. *Cell.* 2006 Nov 17;127(4):831–46.
- 616 22. Mutch S, Kensel-Hammes P, Gadd J, Fujimoto B, Allen R, Schiro P, et al. Protein
617 Quantification at the Single Vesicle Level Reveals That a Subset of Synaptic Vesicle
618 Proteins Are Trafficked with High Precision. *Journal of Neuroscience.* 2011 Jan
619 26;31(4):1461.
- 620 23. Takamori S, Rhee JS, Rosenmund C, Jahn R. Identification of a vesicular glutamate
621 transporter that defines a glutamatergic phenotype in neurons. *Nature.* 2000 Sep
622 14;407(6801):189–94.
- 623 24. Bellocchio EE, Reimer RJ, Fremeau RT, Edwards RH. Uptake of glutamate into
624 synaptic vesicles by an inorganic phosphate transporter. *Science.* 2000 Aug
625 11;289(5481):957–60.
- 626 25. Herzog E, Bellenchi GC, Gras C, Bernard V, Ravassard P, Bedet C, et al. The
627 existence of a second vesicular glutamate transporter specifies subpopulations of
628 glutamatergic neurons. *J Neurosci.* 2001 Nov 8;21(22):RC181.
- 629 26. Fremeau RT, Troyer MD, Pahner I, Nygaard GO, Tran CH, Reimer RJ, et al. The
630 expression of vesicular glutamate transporters defines two classes of excitatory synapse.
631 *Neuron.* 2001 Aug 2;31(2):247–60.
- 632 27. Gras C, Herzog E, Bellenchi GC, Bernard V, Ravassard P, Pohl M, et al. A third
633 vesicular glutamate transporter expressed by cholinergic and serotonergic neurons. *J*
634 *Neurosci.* 2002 Jul 1;22(13):5442–51.
- 635 28. Schäfer MK-H, Varoqui H, Defamie N, Weihe E, Erickson JD. Molecular cloning and
636 functional identification of mouse vesicular glutamate transporter 3 and its expression
637 in subsets of novel excitatory neurons. *J Biol Chem.* 2002 Dec 27;277(52):50734–48.
- 638 29. Schenck S, Wojcik SM, Brose N, Takamori S. A chloride conductance in VGLUT1
639 underlies maximal glutamate loading into synaptic vesicles. *Nat Neurosci.* 2009
640 Feb;12(2):156–62.

- 641 30. Preobraschenski J, Zander J-F, Suzuki T, Ahnert-Hilger G, Jahn R. Vesicular
642 glutamate transporters use flexible anion and cation binding sites for efficient
643 accumulation of neurotransmitter. *Neuron*. 2014 Dec 17;84(6):1287–301.
- 644 31. Eriksen J, Chang R, McGregor M, Silm K, Suzuki T, Edwards RH. Protons Regulate
645 Vesicular Glutamate Transporters through an Allosteric Mechanism. *Neuron*. 2016 Apr
646 27.
- 647 32. Fremeau RT, Voglmaier S, Seal RP, Edwards RH. VGLUTs define subsets of
648 excitatory neurons and suggest novel roles for glutamate. *Trends Neurosci*. 2004 Feb
649 1;27(2):98–103.
- 650 33. Varoqui H, Schäfer MKH, Zhu H, Weihe E, Erickson JD. Identification of the
651 differentiation-associated Na⁺/PI transporter as a novel vesicular glutamate transporter
652 expressed in a distinct set of glutamatergic synapses. *J Neurosci*. 2002;22(1):142–55.
- 653 34. Fremeau RT, Kam K, Qureshi T, Johnson J, Copenhagen DR, Storm-Mathisen J, et al.
654 Vesicular glutamate transporters 1 and 2 target to functionally distinct synaptic release
655 sites. *Science*. 2004 Jun 18;304(5678):1815–9.
- 656 35. Wojcik SM, Rhee JS, Herzog E, Sigler A, Jahn R, Takamori S, et al. An essential role
657 for vesicular glutamate transporter 1 (VGLUT1) in postnatal development and control
658 of quantal size. *Proc Natl Acad Sci USA*. 2004 May 4;101(18):7158–63.
- 659 36. Moechars D, Weston MC, Leo S, Callaerts-Vegh Z, Goris I, Daneels G, et al. Vesicular
660 glutamate transporter VGLUT2 expression levels control quantal size and neuropathic
661 pain. *J Neurosci*. 2006 Nov 15;26(46):12055–66.
- 662 37. Wallén-Mackenzie A, Gezelius H, Thoby-Brisson M, Nygård A, Enjin A, Fujiyama F,
663 et al. Vesicular glutamate transporter 2 is required for central respiratory rhythm
664 generation but not for locomotor central pattern generation. *J Neurosci*. 2006 Nov
665 22;26(47):12294–307.
- 666 38. Vinatier J, Herzog E, Plamont M-A, Wojcik SM, Schmidt A, Brose N, et al. Interaction
667 between the vesicular glutamate transporter type 1 and endophilin A1, a protein
668 essential for endocytosis. *J Neurochem*. 2006 May;97(4):1111–25.
- 669 39. Voglmaier SM, Kam K, Yang H, Fortin DL, Hua Z, Nicoll RA, et al. Distinct
670 endocytic pathways control the rate and extent of synaptic vesicle protein recycling.
671 *Neuron*. 2006 Jul 6;51(1):71–84.
- 672 40. De Gois S, Jeanclos E, Morris M, Grewal S, Varoqui H, Erickson JD. Identification of
673 endophilins 1 and 3 as selective binding partners for VGLUT1 and their co-localization
674 in neocortical glutamatergic synapses: implications for vesicular glutamate transporter
675 trafficking and excitatory vesicle formation. *Cell Mol Neurobiol*. 2006 Jul;26(4-
676 6):679–93.
- 677 41. Weston MC, Nehring RB, Wojcik SM, Rosenmund C. Interplay between VGLUT
678 isoforms and endophilin A1 regulates neurotransmitter release and short-term plasticity.
679 *Neuron*. 2011 Mar 24;69(6):1147–59.
- 680 42. Pan P-Y, Marrs J, Ryan TA. Vesicular Glutamate Transporter 1 orchestrates

- 681 recruitment of other synaptic vesicle cargo proteins during synaptic vesicle recycling. *J*
682 *Biol Chem.* 2015 Jul 29.
- 683 43. Foss SM, Li H, Santos MS, Edwards RH, Voglmaier SM. Multiple Dileucine-like
684 Motifs Direct VGLUT1 Trafficking. *J Neurosci.* 2013 Jun 26;33(26):10647–60.
- 685 44. Li H, Santos MS, Park CK, Dobry Y, Voglmaier SM. VGLUT2 Trafficking Is
686 Differentially Regulated by Adaptor Proteins AP-1 and AP-3. *Front Cell Neurosci.*
687 *Frontiers;* 2017;11.
- 688 45. Siksou L, Silm K, Biesemann C, Nehring RB, Wojcik SM, Triller A, et al. A role for
689 vesicular glutamate transporter 1 in synaptic vesicle clustering and mobility. *Eur J*
690 *Neurosci.* 2013 May;37(10):1631–42.
- 691 46. Herman MA, Ackermann F, Trimbuch T, Rosenmund C. Vesicular glutamate
692 transporter expression level affects synaptic vesicle release probability at hippocampal
693 synapses in culture. *J Neurosci.* 2014 Aug 27;34(35):11781–91.
- 694 47. Martineau M, Guzman RE, Fahlke C, Klingauf J. VGLUT1 functions as a
695 glutamate/proton exchanger with chloride channel activity in hippocampal
696 glutamatergic synapses. *Nat Commun.* 2017 Dec 22;8(1):2279.
- 697 48. Qi YB, Garren EJ, Shu X, Tsien RY, Jin Y. Photo-inducible cell ablation in
698 *Caenorhabditis elegans* using the genetically encoded singlet oxygen generating protein
699 miniSOG. *Proc Natl Acad Sci USA.* 2012 May 8;109(19):7499–504.
- 700 49. Berger A, Lorain S, Joséphine C, Desrosiers M, Peccate C, Voit T, et al. Repair of
701 rhodopsin mRNA by spliceosome-mediated RNA trans-splicing: a new approach for
702 autosomal dominant retinitis pigmentosa. *Mol Ther.* 2015 May;23(5):918–30.
- 703 50. Markwardt ML, Kremers G-J, Kraft CA, Ray K, Cranfill PJC, Wilson KA, et al. An
704 improved cerulean fluorescent protein with enhanced brightness and reduced reversible
705 photoswitching. *PLoS ONE.* 2011;6(3):e17896.
- 706 51. Bardy C, van den Hurk M, Eames T, Marchand C, Hernandez RV, Kellogg M, et al.
707 Neuronal medium that supports basic synaptic functions and activity of human neurons
708 *in vitro.* *Proc Natl Acad Sci USA.* 2015 May 19;112(20):E2725–34.
- 709 52. McAnaney TB, Zeng W, Doe CFE, Bhanji N, Wakelin S, Pearson DS, et al.
710 Protonation, photobleaching, and photoactivation of yellow fluorescent protein (YFP
711 10C): a unifying mechanism. *Biochemistry.* 2005 Apr 12;44(14):5510–24.
- 712 53. Rasband WS. ImageJ, U.S. National Institutes of Health, Bethesda, Maryland, USA.
713 <http://rsb.info.nih.gov/ij/>. 1997.
- 714 54. Zala D, Hinckelmann M-V, Yu H, Lyra da Cunha MM, Liot G, Cordelières FP, et al.
715 Vesicular Glycolysis Provides On-Board Energy for Fast Axonal Transport. *Cell.* 2013
716 Jan;152(3):479–91.
- 717 55. Kinoshita E, Kinoshita-Kikuta E, Takiyama K, Koike T. Phosphate-binding tag, a new
718 tool to visualize phosphorylated proteins. *Mol Cell Proteomics.* 2006 Apr;5(4):749–57.

- 719 56. Almqvist, Huang, Laaksonen, Wang, Hovmöller. Docking and homology modeling
720 explain inhibition of the human vesicular glutamate transporters. *Protein Sci.* 2007 Jul
721 27.
- 722 57. Juge N, Yoshida Y, Yatsushiro S, Omote H, Moriyama Y. Vesicular glutamate
723 transporter contains two independent transport machineries. *J Biol Chem.* 2006 Dec
724 22;281(51):39499–506.
- 725 58. Miyazaki T, Fukaya M, Shimizu H, Watanabe M. Subtype switching of vesicular
726 glutamate transporters at parallel fibre-Purkinje cell synapses in developing mouse
727 cerebellum. *Eur J Neurosci.* 2003 Jun 1;17(12):2563–72.
- 728 59. Herzog E, Takamori S, Jahn R, Brose N, Wojcik SM. Synaptic and vesicular co-
729 localization of the glutamate transporters VGLUT1 and VGLUT2 in the mouse
730 hippocampus. *J Neurochem.* 2006 Nov;99(3):1011–8.
- 731 60. Schuske K, Jorgensen EM. Neuroscience. Vesicular glutamate transporter--shooting
732 blanks. *Science.* 2004 Jun 18;304(5678):1750–2.
- 733 61. Pechstein A, Gerth F, Milosevic I, Jäpel M, Eichhorn-Grünig M, Vorontsova O, et al.
734 Vesicle uncoating regulated by SH3-SH3 domain-mediated complex formation
735 between endophilin and intersectin at synapses. *EMBO Rep.* 2015 Feb;16(2):232–9.
- 736 62. Goh GY, Huang H, Ullman J, Borre L, Hnasko TS, Trussell LO, et al. Presynaptic
737 regulation of quantal size: K(+)/H(+) exchange stimulates vesicular glutamate transport.
738 *Nat Neurosci.* 2011 Aug 28.
- 739 63. Hilfiker S, Pieribone VA, Czernik AJ, Kao HT, Augustine GJ, Greengard P. Synapsins
740 as regulators of neurotransmitter release. *Philos Trans R Soc Lond, B, Biol Sci.* 1999
741 Feb 28;354(1381):269–79.
- 742 64. Evergren E, Gad H, Walther K, Sundborger A, Tomilin N, Shupliakov O. Intersectin is
743 a negative regulator of dynamin recruitment to the synaptic endocytic zone in the
744 central synapse. *J Neurosci.* 2007 Jan 10;27(2):379–90.
- 745 65. Milosevic I, Giovedi S, Lou X, Raimondi A, Collesi C, Shen H, et al. Recruitment of
746 endophilin to clathrin-coated pit necks is required for efficient vesicle uncoating after
747 fission. *Neuron.* 2011 Nov 17;72(4):587–601.
- 748 66. Farsi Z, Gowrisankaran S, Krunic M, Rammner B, Woehler A, Lafer EM, et al.
749 Clathrin coat controls synaptic vesicle acidification by blocking vacuolar ATPase
750 activity. *eLife.* eLife Sciences Publications Limited; 2018 Apr 13;7:e32569.
- 751 67. Santos MS, Foss SM, Park CK, Voglmaier SM. Protein Interactions of the Vesicular
752 Glutamate Transporter VGLUT1. *PLoS ONE.* 2014;9(10):e109824.
- 753 68. Richter K, Schmutz I, Darna M, Zander J-F, Chavan R, Albrecht U, et al. VGLUT1
754 binding to endophilin or intersectin1 and dynamin phosphorylation in a diurnal context.
755 *Neuroscience.* 2017 Nov 30.
- 756 69. Gerth F, Jäpel M, Pechstein A, Kochlamazashvili G, Lehmann M, Puchkov D, et al.
757 Intersectin associates with synapsin and regulates its nanoscale localization and

- 758 function. *Proc Natl Acad Sci USA*. 2017 Oct 23;85:201715341.
- 759 70. Winther ÅME, Vorontsova O, Rees KA, Näreoja T, Sopova E, Jiao W, et al. An
760 Endocytic Scaffolding Protein together with Synapsin Regulates Synaptic Vesicle
761 Clustering in the *Drosophila* Neuromuscular Junction. *J Neurosci*. 2015 Nov
762 4;35(44):14756–70.
- 763 71. Humphries AC, Donnelly SK, Way M. Cdc42 and the Rho GEF intersectin-1
764 collaborate with Nck to promote N-WASP-dependent actin polymerisation. *J Cell Sci*.
765 2014 Feb 1;127(Pt 3):673–85.
- 766 72. Wilson NR, Kang J, Hueske EV, Leung T, Varoqui H, Murnick JG, et al. Presynaptic
767 regulation of quantal size by the vesicular glutamate transporter VGLUT1. *J Neurosci*.
768 2005 Jun 29;25(26):6221–34.
- 769 73. De Gois S, Schäfer MK-H, Defamie N, Chen C, Ricci A, Weihe E, et al. Homeostatic
770 scaling of vesicular glutamate and GABA transporter expression in rat neocortical
771 circuits. *J Neurosci*. 2005 Aug 3;25(31):7121–33.
- 772 74. Rothman JS, Kocsis L, Herzog E, Nusser Z, Silver RA. Physical determinants of
773 vesicle mobility and supply at a central synapse. *eLife*. 2016 Aug 19;5.
- 774 75. Patzke C, Brockmann MM, Dai J, Gan KJ, Grauel MK, Fenske P, et al.
775 Neuromodulator Signaling Bidirectionally Controls Vesicle Numbers in Human
776 Synapses. *Cell*. 2019 179: 498–513.e22
- 777

778
779
780

TABLES

| | Mutation | Domain/Motif | Name | putative function |
|--------|---------------------------------------|--------------------------|----------------------------|--|
| VGLUT1 | R80Q/R176K/R314Q | TM1;TM4;TM7 | sVGLUT1 | Glutamate transport |
| | Δ504-560 | Whole C-terminus | ΔC-term | SV/VGLUT Trafficking |
| | DQL514AQA | PDZ type 3 binding | DQL514AQA | Unknown |
| | Δ530-560 | Proline Rich Domains 1+2 | ΔPRD1+2 | SH3 domain binding |
| | PP534AA | Proline Rich Domain1 | PP534AA | SH3 domain binding |
| | S540A | SYGAT | S540A | Unknown |
| | T544A | SYGAT | T544A | Unknown |
| | Δ550-560 | Proline Rich Domain 2 | ΔPRD2 | Endophilin binding |
| P554A | Proline Rich Domain 2 | P554A | Endophilin binding | |
| | EndoA1 290-352 | SH3 | SH3 | Binds PRD and ITSN1 SH3B |
| | EndoA1 290-352 ^{E329K,S336K} | SH3 | SH3 ^{E329K,S336K} | Binds PRD and ITSN1 SH3B |
| | ITSN1 903-971 | SH3B | SH3B | Endo SH3 binding through E329 and S336 |

781
782
783

Table 1: List of mutant constructs tested.

784
785
786
787
788

FIGURE LEGENDS

Figure 1: Dose dependent regulation of SV super-pool size by VGLUT1.

789 A: Expression of Synaptobrevin2 fused to Enhanced Green Fluorescent Protein (Syn2^{EGFP}) in
790 hippocampal neurons at 18 days in culture. B: examples of FRAP sequences from both
791 *Slc17a7* (VGLUT1) *+/+* and *-/-* genotypes. Boutons are imaged for 3 min, bleached, and
792 recovery is recorded for 73 min. C: average FRAP kinetics. 27 synapses from *+/+* and 31
793 synapses from *-/-* were measured by FRAP and the average traces are displayed here (for *+/+*
794 $N = 8$ cultures; for *-/-* $N = 11$ cultures). The two traces were fitted using double exponential
795 components equations and the convergence of the traces to a common fit was tested using the
796 extra sum of squares F test. The F test indicates that the traces are best fitted by 2 divergent
797 models (F ratio = 19.32; $P < 0.0001$). Fast FRAP recovery was monitored every 5 s in an
798 independent set of experiments (inset). D: Expression of transduced VGLUT1^{venus} in
799 hippocampal neurons. E: Average FRAP recovery of VGLUT1^{venus} at 68 minutes post-bleach
800 in rescue or over-expression. Over-expression reduces the mobility of SVs (Unpaired t test, P
801 = 0.0385, $t = 2.176$. For overexpression: $N = 4$ cultures, $n = 14$ synapses; for rescue: $N = 3$
802 cultures, $n = 15$ synapses). scale bar: 2 μ m in A and D, 1 μ m in B.

803

804 **Figure 2:** Structure of VGLUT1 and expression of mutants in neurons.

805 A: schematic of VGLUT1 structure with 560 amino acids, 12 transmembrane domains, N-
806 and C-termini facing the cytoplasmic side, and N-glycosylation at the first luminal loop. In
807 blue the 3 residues mutated to silence VGLUT1 transport (sVGLUT1 see Figure3). Red bars
808 mark the 3 deletions used (Δ C-term, Δ PRD1+2, Δ PRD2). Red residues were mutated to
809 alanine in order to test their role in the super-pool regulation supported by VGLUT1. All
810 mutations carried a venus tag at the C-terminus. B: examples of expression patterns obtained
811 with VGLUT1 WT and mutants upon transduction in hippocampal neurons matching
812 endogenous expression levels. Note the dense punctate expression and low somatic signal
813 typical of VGLUT1 distribution. Scale bar 10 μ m. C: Measurement of bouton area. None of
814 the mutants displayed a shift in bouton size compared to WT controls. D: Measurement of
815 fluorescence intensity. None of the mutants displayed a significant shift in fluorescence
816 intensity compared to WT controls.

817

818 **Figure 3:** Glutamate transport and SV tonicity are not involved in the reduction of SV super-
819 pool size.

820 A: Expression of VGLUT1^{mCherry}, sVGLUT1^{mCherry} and Syb2^{EGFP} in hippocampal neurons.
821 FRAP was performed on Syb2^{EGFP} at axons, both on those with, and those without mCherry
822 signal. Scale bar 5 μ m. B: Average FRAP kinetics from knock-out cells rescued by
823 VGLUT1^{mCherry}, sVGLUT1^{mCherry}, and VGLUT1 KO synapses not rescued. Synapses from
824 each genotype were measured by FRAP and the average traces are displayed ($N = 7$
825 independent cultures, 16 synapses for -/-; $N = 5$ cultures, 23 synapses for WT rescue, and $N =$
826 10 cultures, 36 synapses for sVGLUT1 rescue). The 3 traces were fitted using double
827 exponential components equations and the convergence of the traces to a common fit was
828 tested using the extra sum of squares F test. The F test indicates that the traces are best fitted
829 by 2 divergent models (one for -/- synapses and the other one for both rescues, F ratio =
830 30.25; $P < 0.0001$). FRAP kinetics for the 2 types of rescued synapses are best fitted by one
831 convergent model (F ratio = 1.235; $P = 0.294$). C: Spontaneous excitatory activity in
832 VGLUT1 KO rescued neurons. Example traces of mEPSC activity in wild type and
833 sVGLUT1 rescue conditions. D: Comparison of the amplitude of mEPSC events in wild type
834 and sVGLUT1 rescue conditions ($N=3$ independent cultures, $n=31$ cells, mean
835 amplitude=15.3 pA \pm 1.15 SEM for wild type rescue; $N = 3$ independent cultures, $n=56$ cells,
836 mean amplitude = 13.12 pA \pm 0.71SEM for sVGLUT1 rescue; unpaired t-test $P = 0.011$). E:
837 Comparison of the frequency of mEPSC events in wild type and sVGLUT1 rescue conditions.
838 ($N = 3$ independent cultures, $n=31$ cells, mean frequency= 3.51 Hz \pm 0.6 SEM for wild type
839 rescue; $N = 3$ independent cultures, $n=56$ cells, mean frequency = 2.51 Hz \pm 0.58 SEM for
840 sVGLUT1 rescue; unpaired t-test $P = 0.008$). Note that sVGLUT1 conditions are both
841 significantly smaller than wild type rescue conditions.

842

843 **Figure 4:** The VGLUT1 PRD2 domain mediates SV super-pool size and mEPSC frequency
844 reductions

845 A: Comparison of VGLUT1^{venus} and VGLUT1^{P554A-venus} rescues of VGLUT1 KO on SV
846 exchange rates at synapses. 21 (WT) and 22 (P554A) synapses from each rescue were
847 measured by FRAP and the average traces are displayed ($N = 5$ cultures for WT and $N = 5$
848 cultures for P554A). The two traces were fitted using double exponential components
849 equations and the convergence of the traces to a common fit was tested using the extra sum of
850 squares F test. The F test indicates that the traces are best fitted by 2 divergent models (F ratio
851 = 19.64; $P < 0.0001$). B: Similar experiments where performed for Δ PRD1+2, Δ PRD2,

852 DQL514AQA, PP534AA, S540A and T544A. The results are displayed here as a comparison
853 of fluorescence recovery to the corresponding WT control 68 min after bleaching. Only
854 mutants affecting PRD2 display a lack of reduction to WT levels and a significantly higher
855 SV exchange rate (*t* test, WT vs. Δ PRD1+2: $P = 0.0005$, $t = 3.790$; vs. Δ PRD2: $P < 0.0001$, t
856 $= 4.369$; vs. P554A: $P = 0.0293$, $t = 2.266$). C: Time lapse imaging of SV axonal transport.
857 VGLUT1^{venus}, or VGLUT1^{P554A-venus}, or VGLUT1^{S540A-venus} were expressed in VGLUT1 KO
858 neurons. Example sequence extracted from the boxed fiber (left) sampled every 200ms over
859 30s (middle). Vertical arrowhead points to a venus fluorescent dot traveling along the axon.
860 Kymograph of fluorescence movements within the example fiber (boxed in middle panel).
861 Vertical arrowhead points to the same traced event shown in the middle panel. Scale bar: left
862 5 μ m, middle 2 μ m. D: Cumulative axonal fluorescence traffic measured over time-lapse
863 sequences. A significant increase in VGLUT1^{venus} traffic is seen when P554A is expressed
864 compared to WT and S540A mutant (unpaired *t* test, WT vs. P554A: $P = 0.0092$, $t = 3.564$; vs.
865 S540A: $P = 0.8963$, $t = 0.1351$. $N = 5$ cultures for WT, and $N = 4$ cultures for both P554A and
866 S540A.). E: Average speed of VGLUT1^{venus} dots was extracted from kymographs. No
867 significant changes in speed was seen for mutants tested compared to WT (One-way ANOVA,
868 $P = 0.0634$, F ratio = 2.431. Speed for each mutant, WT: 1.564 ± 0.02692 μ m/s; P554A:
869 1.536 ± 0.02860 μ m/s; S540A: 1.460 ± 0.02942 μ m/s). F: Spontaneous excitatory activity in
870 VGLUT1 KO neurons rescued by wild type and P554A VGLUT1 constructs. Example traces
871 of mEPSC activity in sham controls, wild type and VGLUT1^{P554A} rescue conditions. G:
872 Comparison of the amplitude of mEPSC events in wild type and VGLUT1^{P554A} rescue
873 conditions ($N = 3$ independent cultures, $n=53$ cells, mean amplitude= 12.73 pA ± 0.79 SEM
874 for sham controls; $N = 3$ independent cultures, $n=61$ cells, mean amplitude= 16.05 pA ± 1.05
875 SEM for wild type rescue; $N = 3$ independent cultures, $n=53$ cells, mean amplitude = 15.59
876 pA ± 1.02 SEM for *vglut1*^{P554A} rescue; Mann-Whitney test of wild type versus VGLUT1^{P554A},
877 $P=0.485$). Note that both wild type and VGLUT1^{P554A} rescue mEPSC amplitudes significantly
878 and to the same extent compared to sham controls. H: Comparison of the frequency of
879 mEPSC events in wild type and VGLUT1^{P554A} rescue conditions ($N = 3$ independent cultures,
880 $n=53$ cells, mean frequency= 2.14 Hz ± 0.37 SEM for sham controls; $N = 3$ independent
881 cultures, $n=61$ cells, mean frequency= 5.53 Hz ± 0.87 SEM for wild type rescue; $N = 3$
882 independent cultures, $n=53$ cells, mean frequency = 7.59 Hz ± 0.97 SEM for VGLUT1^{P554A}
883 rescue; Mann-Whitney test of wild type versus VGLUT1^{P554A}, $P=0.031$). Note that
884 VGLUT1^{P554A} mEPSC events are significantly more frequent than wild type rescue conditions.
885 I: Comparison of the frequency of mIPSC events in wild type and VGLUT1^{P554A} rescue

886 conditions ($N = 3$ independent cultures, $n=53$ cells, mean frequency= $6.21\text{Hz} \pm 0.69$ SEM for
 887 sham controls; $N = 3$ independent cultures, $n=61$ cells, mean frequency= $7.28 \text{ Hz} \pm 0.69$ SEM
 888 for wild type rescue; $N = 3$ independent cultures, $n=53$ cells, mean frequency = $6.79 \text{ Hz} \pm$
 889 0.63 SEM for VGLUT1^{P554A} rescue; Mann-Whitney test of wild type versus VGLUT1^{P554A},
 890 $P=0.781$). Note that all groups are equivalent regarding mIPSC amplitudes (Figure 4-figure
 891 supplement 2 displays the full IPSC data set). J: Post-hoc analysis of VGLUT1^{venus} average
 892 fluorescence integrated intensity at boutons in cultures monitored in electrophysiology. ($N = 2$
 893 independent cultures, mean integrated intensity of punctate VGLUT1^{venus} signal= $3.28 \text{ AU} \pm$
 894 0.15 SEM for wild type rescue; $N = 2$ independent cultures, mean integrated intensity of
 895 punctate VGLUT1^{venus} signal = $3.11 \text{ AU} \pm 0.31$ SEM for VGLUT1^{P554A} rescue; T test,
 896 $P=0.348$).

897

898 **Figure 5:** A tripartite complex between VGLUT1, endophilinA1 and intersectin1 mediates
 899 SV super-pool reduction.

900 A: Schematic model of the competition experiment designed to test for the effective
 901 recruitment of intersectin1 at the VGLUT1/endophilinA1 complex (61). The three SH3
 902 domains over-expressed in this competition assay disrupt distinct parts of the tripartite
 903 complex. The SH3 domain of endophilinA1 displaces the endogenous endophilinA1 BAR
 904 domain (Endo SH3^{WT}). The SH3 domain of endophilinA1 mutated at E329K and S336K
 905 disrupts the interaction of intersectin1 with the VGLUT1/endophilinA1 complex(61). Finally,
 906 the SH3B domain of intersectin1 should displace the endogenous intersectin1 and allows us to
 907 assess whether the full-length intersectin1 is required. B: Over-expression of SH3 domains
 908 fused with mCerulean3 in VGLUT1^{venus} neurons. Axons filled with mCerulean3 were
 909 selected for FRAP experiments. Scale bar $2\mu\text{m}$. C: FRAP measurement of SV super-pool in
 910 SH3 domains competition experiments. Synapses from each over-expression condition were
 911 measured by FRAP and the average recovery after 68 minutes are displayed ($0.5346 \pm$
 912 0.04128 , $N=4$ and $n=20$ for sham; 0.6071 ± 0.03705 , $N=5$ and $n=25$ for Endo-SH3^{WT}; 0.7323
 913 ± 0.04909 , $N=4$ and $n=18$ for Endo-SH3^{E329K,S336K}; 0.6894 ± 0.04036 , $N=5$ and $n=25$ for
 914 ITSN1-SH3B). Sham and Endo-SH3^{WT} converged to a lower SV exchange recovery (Mann-
 915 Whitney test, $P=0.141$) while Endo-SH3^{E329K,S336K} (Mann-Whitney test, $P=0.005$ **) and
 916 ITSN1-SH3B (Mann-Whitney test, $P=0.014$ *) generated higher SV exchange recovery
 917 curves.

918

919 **Supporting Information :**

920 **Figure 1-figure supplement 1:** VGLUT2 does not rescue SV super-pool size in VGLUT1
 921 knock out neurons.

922 A: Average FRAP kinetics obtained upon rescue of VGLUT1 KO cells by either
 923 VGLUT1^{venus} or VGLUT2^{venus} lentivirus. 24 synapses from VGLUT1^{venus} and 20 synapses
 924 from VGLUT2^{venus} were measured by FRAP and the average traces are displayed
 925 (VGLUT1^{venus} rescue $N = 7$ culture VGLUT2^{venus} $N = 7$ cultures). The two traces were fitted
 926 using double exponential components equations and the convergence of the traces to a
 927 common fit was tested using the extra sum of squares F test. The F test indicates that the
 928 traces are best fitted by 2 divergent models (F ratio = 19.27 ; $P < 0.0001$).

929

930 **Figure 3-figure supplement 1:** VGLUT2 expression diminishes in hippocampal neurons
 931 until DIV17

932 A: Immunofluorescence of VGLUT2 on hippocampal neurons at DIV 6, 12, 17, and 22. Scale
 933 bar 40 μ m. B: Quantification of VGLUT2 expression during hippocampal neuron culture
 934 development. Note the 3-fold reduction of VGLUT2 level between DIV 6 and 17, while the
 935 expression reached a low plateau between DIV17 and 22. DIV6, $N=4$, mean intensity =
 936 612.8 ± 53.8 ; DIV12, $N=3$, mean intensity = 325.9 ± 39.0 ; DIV17, $N=7$, mean intensity =
 937 202.8 ± 8.2 ; DIV22, $N=5$, mean intensity = 191.2 ± 24.2 . One way ANOVA $p \leq 0.001$; pair
 938 wise comparisons: DIV6 vs. DIV22 $p < 0,001$; DIV6 vs. DIV17 $p < 0,001$; DIV6 vs. DIV12 p
 939 $< 0,001$; DIV12 vs. DIV22 $p = 0,044$; DIV12 vs. DIV17 $p = 0,052$; DIV17 vs. DIV22 $p = 0,989$

940

941 **Figure 3-figure supplement 2:** Vesicular glutamate uptake function does not influence
 942 mIPSCs features.

943 A. Spontaneous inhibitory activity in VGLUT1 KO rescued neurons. Example traces of
 944 mIPSC activity in wild type and sVGLUT1 rescue conditions. B: Comparison of the
 945 frequency of mIPSC events in wild type and sVGLUT1 rescue conditions ($N = 3$ independent
 946 cultures, $n=31$ cells, mean frequency = $4.08 \text{ Hz} \pm 0.59 \text{ SEM}$ for wild type rescue; $N = 3$
 947 independent cultures, $n=56$ cells, mean frequency = $3.99 \text{ Hz} \pm 0.52 \text{ SEM}$ for sVGLUT1
 948 rescue; unpaired t-test $P = 0.62$). C: Comparison of the amplitude of mIPSC events in wild
 949 type and sVGLUT1 rescue conditions ($N = 3$ independent cultures, $n=31$ cells, mean
 950 amplitude = $18.06 \text{ pA} \pm 1.07 \text{ SEM}$ for wild type rescue; $N = 3$ independent cultures, $n=56$ cells,
 951 mean amplitude = $17.69 \text{ pA} \pm 0.73 \text{ SEM}$ for sVGLUT1 rescue; unpaired t-test $P = 0.70$).

952

953 **Figure 4-figure supplement 1:** VGLUT1 is phosphorylated but not at the conserved 540-
954 SYGAT motif

955 A: Effect of alkaline phosphatase on the electrophoretic mobility of VGLUT1 from forebrain
956 homogenates (and positive control VIAAT ; Vesicular Inhibitory Amino-Acid Transporter).

957 B: regional distribution of VGLUT1 phosphorylation state. Homogenates of several brain
958 regions where probed for VGLUT1 signal as in panel A. OB: olfactory bulb, St: Striatum,

959 Hipp: Hippocampus, BS: Brain Stem, Thal: Thalamus, Cb: Cerebellum, Cx: Cortex. C:

960 PhosTag assay on VGLUT1 KO primary neuron cultures rescued with VGLUT1^{venus} WT and

961 C-terminal mutant constructs. Note that PhosTag assays prevent from using a size ladder. All
962 constructs display a phospho-shifted band that disappeared upon desphosphorylation by

963 alkaline phosphatase. PI : phosphatase inhibitors; AP: alkaline phosphatase. Selected lanes

964 blotted on the same membranes were reorganized for display purpose.

965

966 **Figure 4-figure supplement 2:** VGLUT1 PRD2 domain removal does not affect mIPSCs

967 features.

968 A: Spontaneous inhibitory activity in VGLUT1 KO neurons rescued by wild type and
969 VGLUT1 P554A constructs. Example traces of mIPSC activity in sham controls, wild type

970 and VGLUT1^{P554A} rescue conditions. B: Comparison of the frequency of mIPSC events in

971 wild type and VGLUT1^{P554A} rescue conditions ($N = 3$ independent cultures, $n=53$ cells, mean

972 frequency= $6.21 \text{ Hz} \pm 0.69 \text{ SEM}$ for sham controls; $N = 3$ independent cultures, $n=61$ cells,

973 mean frequency= $7.28 \text{ Hz} \pm 0.69 \text{ SEM}$ for wild type rescue; $N = 3$ independent cultures, $n=53$

974 cells, mean frequency = $6.79 \text{ Hz} \pm 0.63 \text{ SEM}$ for VGLUT1^{P554A} rescue; Mann-Whitney test of

975 wild type versus VGLUT1^{P554A}, $P=0.781$). C: Comparison of the amplitude of mIPSC events

976 in wild type and VGLUT1^{P554A} rescue conditions ($N = 3$ independent cultures, $n=53$ cells,

977 mean amplitude= $19.29 \text{ pA} \pm 1.34 \text{ SEM}$ for sham controls; $N = 3$ independent cultures, $n=61$

978 cells, mean amplitude= $22.47 \text{ pA} \pm 1.13 \text{ SEM}$ for wild type rescue; $N = 3$ independent cultures,

979 $n=53$ cells, mean amplitude = $19.24 \text{ pA} \pm 0.78 \text{ SEM}$ for VGLUT1^{P554A} rescue; Mann-

980 Whitney test of wild type versus VGLUT1^{P554A}, $P=0.137$).

981

982 **Figure 5-figure supplement 1:** EndophilinA1 accumulates at synaptic vesicle clusters of

983 VGLUT1 synapses.

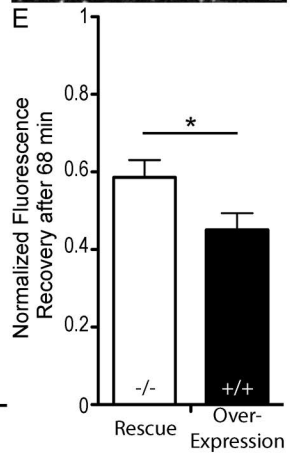
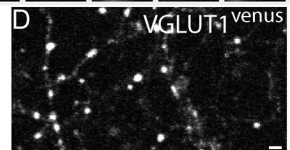
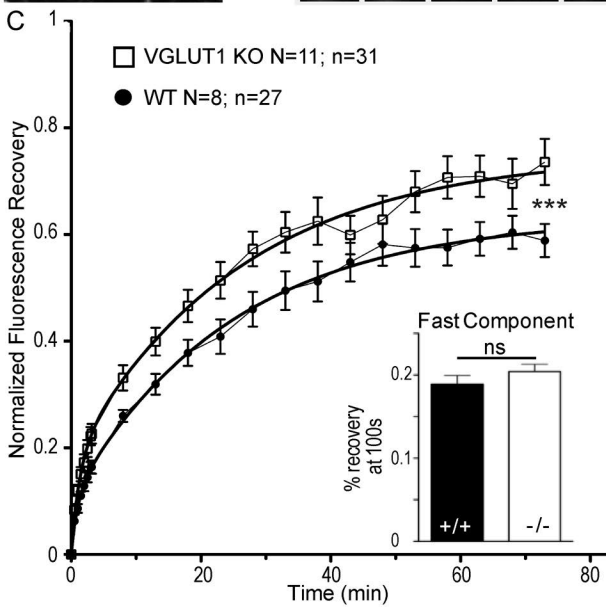
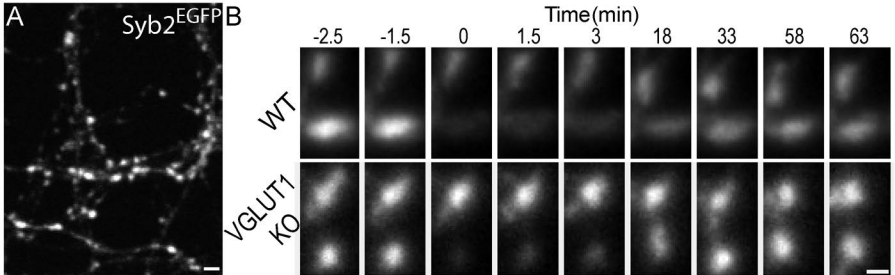
984 Subcellular distribution of EndophilinA1 in VGLUT1 immunopositive terminals in mossy
985 fiber terminals of the cerebellum (A,B) and cortico-striatal projections (C,D). We used pre-
986 embedding immunogold (EndophilinA1) combined with immunoperoxidase (VGLUT1)
987 methods. VGLUT1 immunoreaction product was visible at the level of SV throughout the
988 axoplasm of the terminals. Immunoparticles for EndophilinA1 are detected throughout the
989 axoplasm all over the clusters of VGLUT1 immunopositive vesicles. Scale bar : 500nm

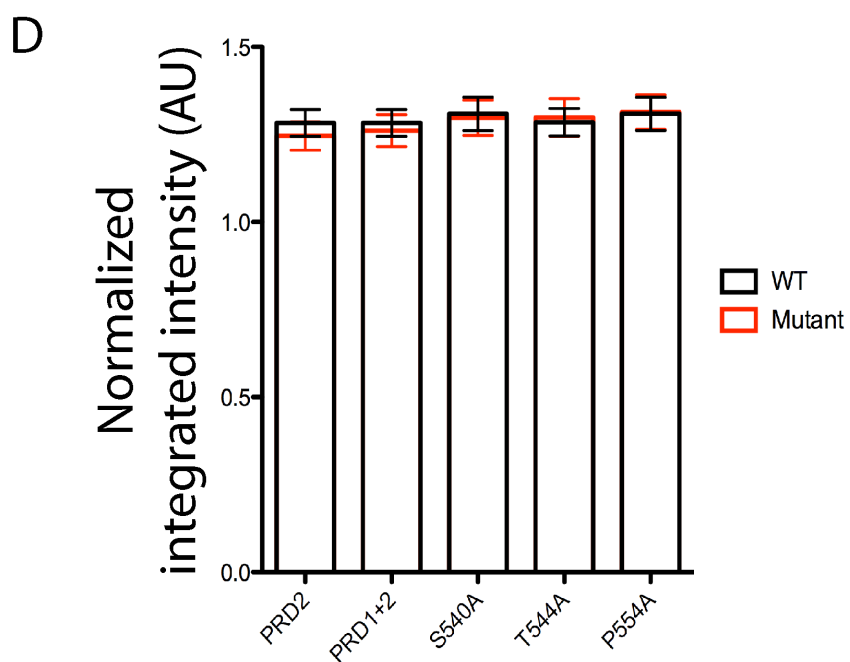
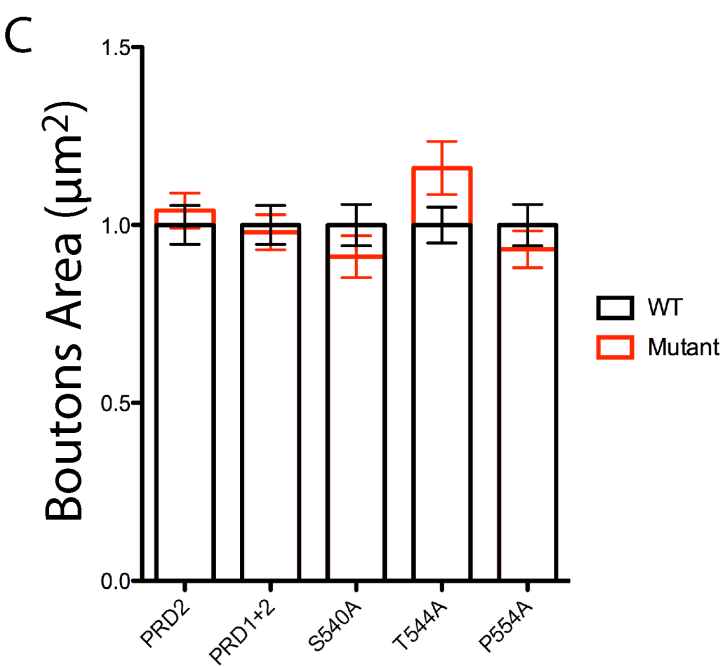
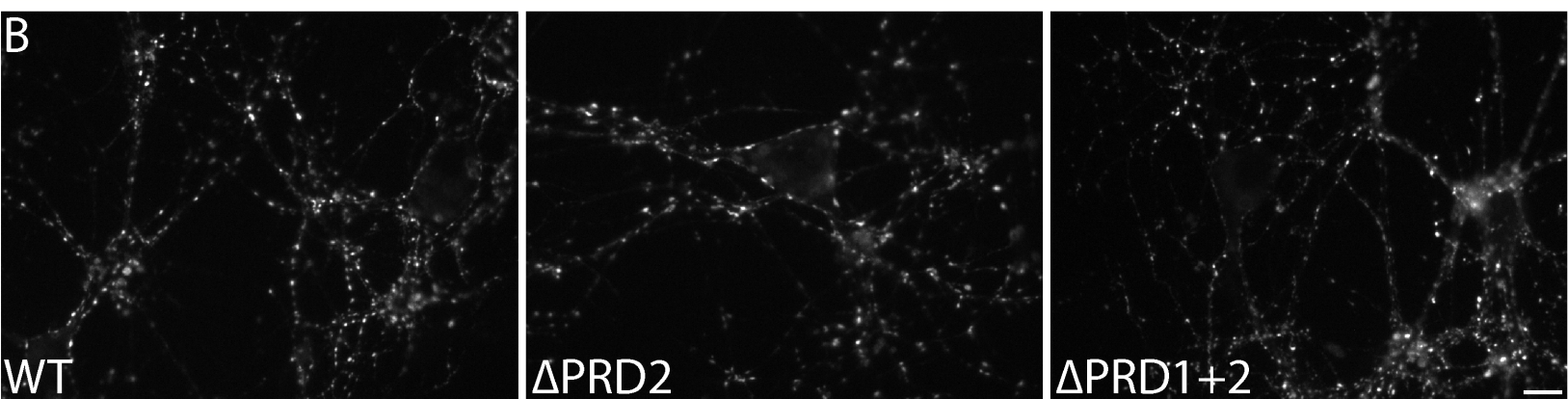
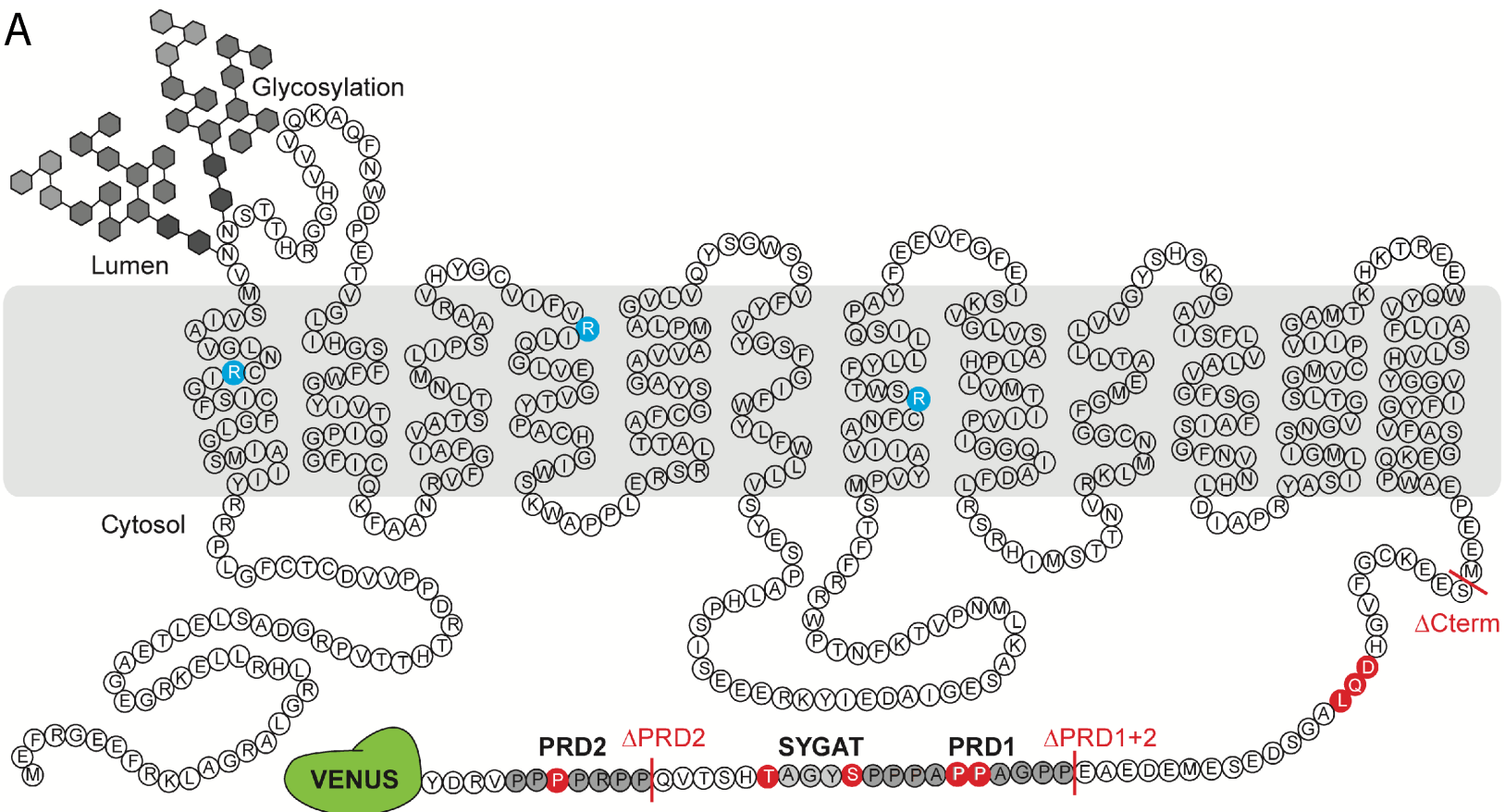
990

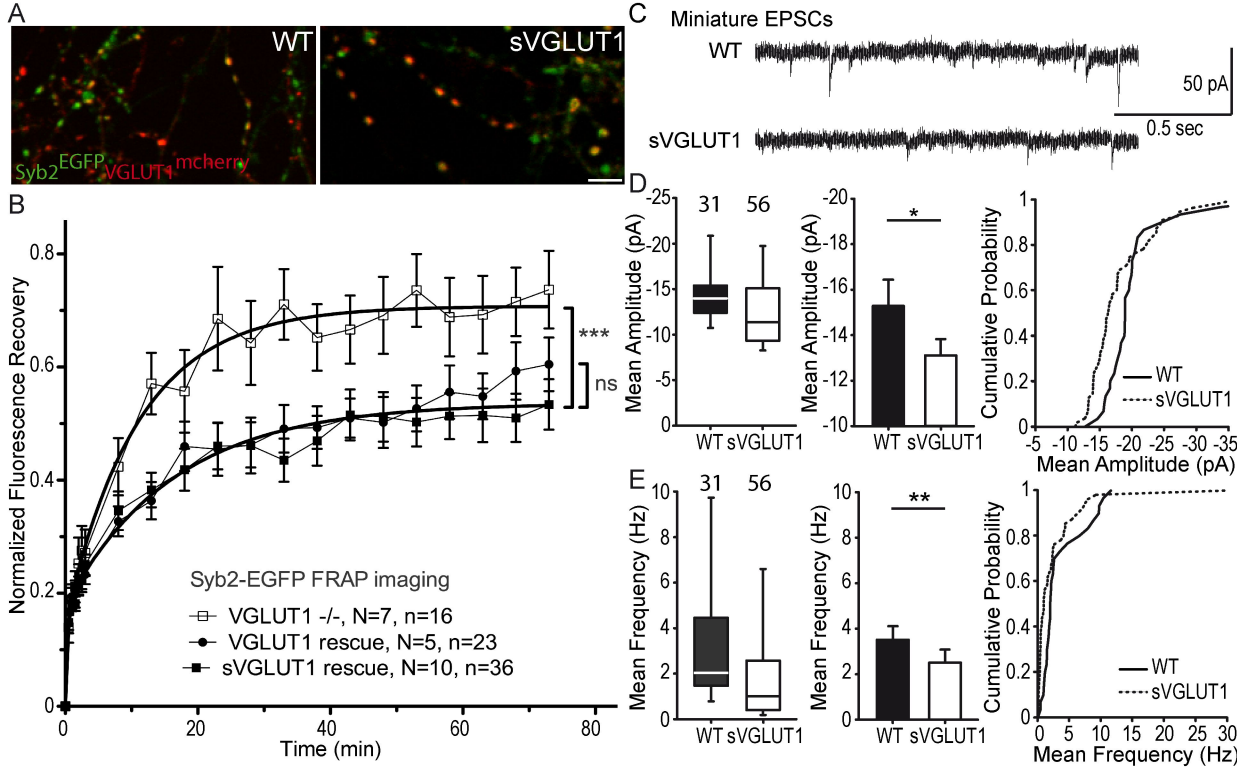
991 **Supplementary file 1:** Supplementary tables collating statistical analysis.

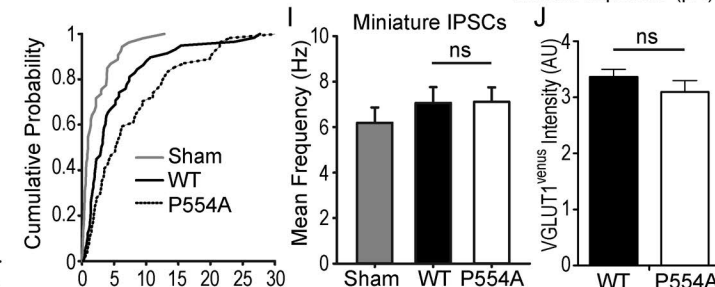
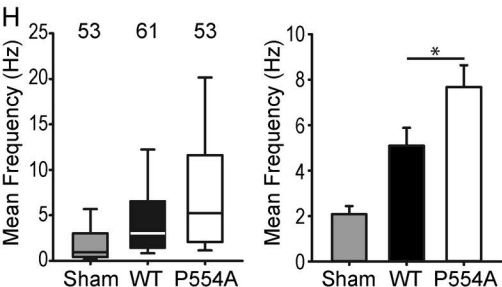
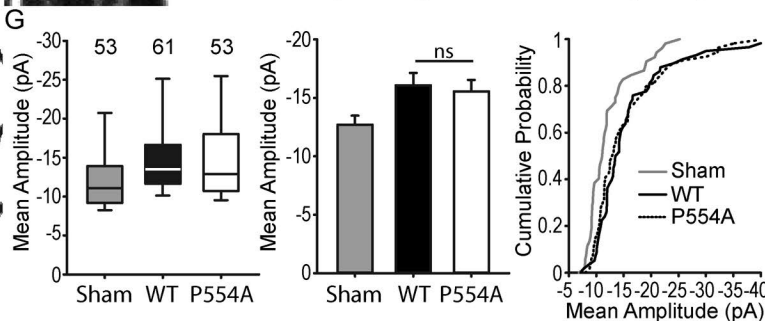
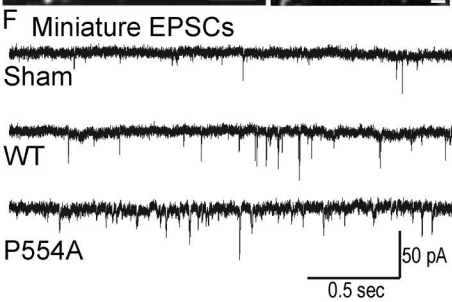
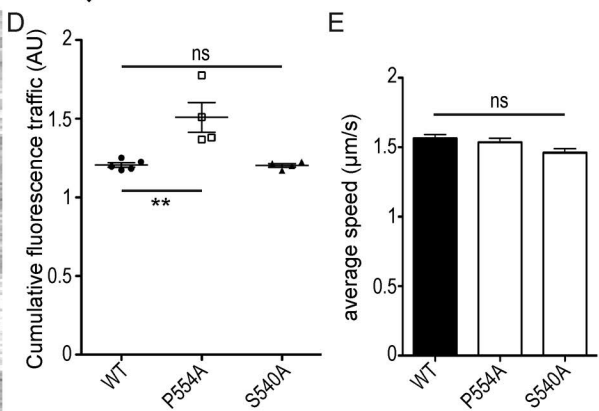
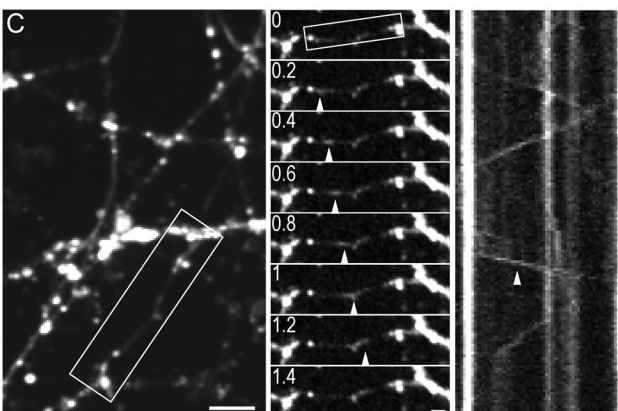
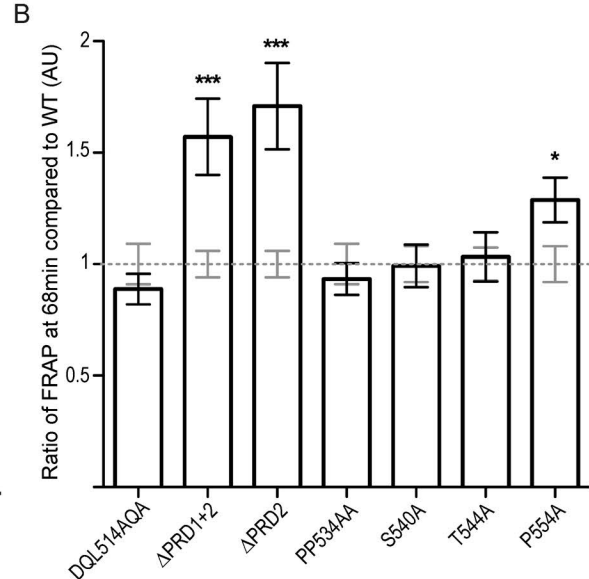
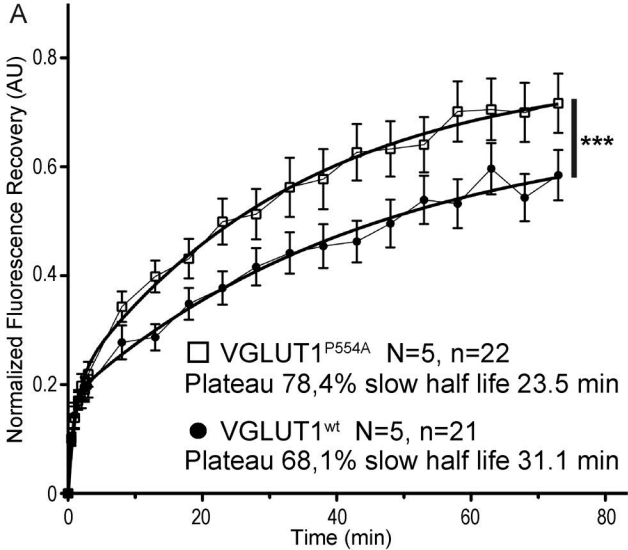
992

993 **Supplementary file 2:** Seal test recording of every cell in the electrophysiology analysis.

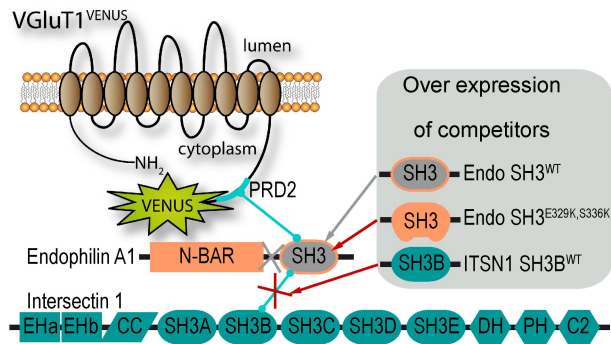




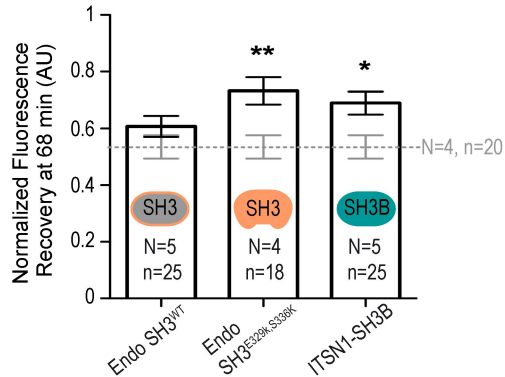




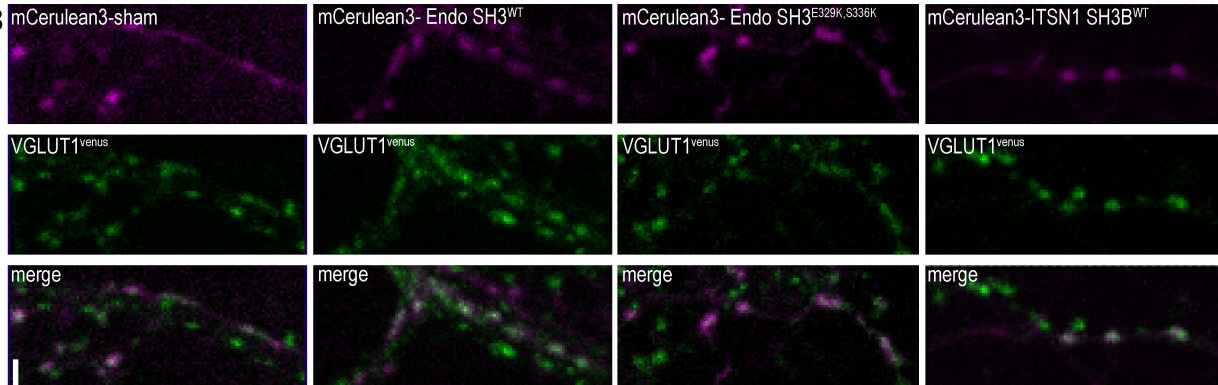
A

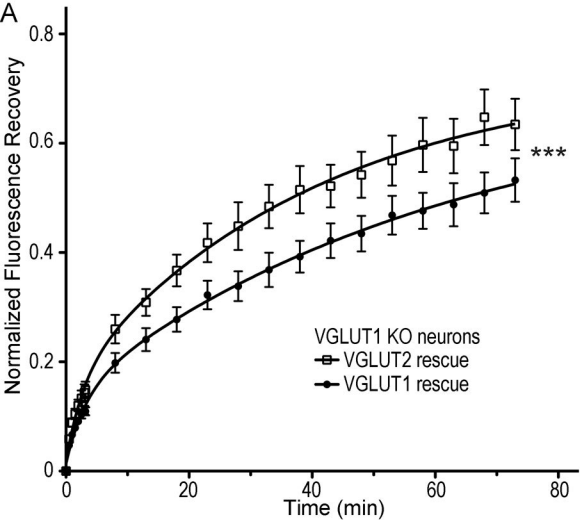


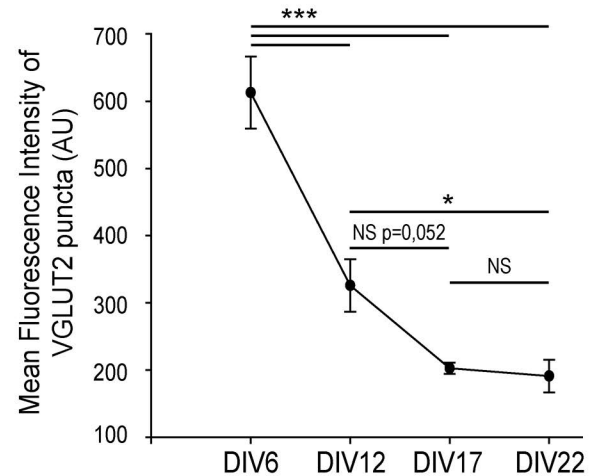
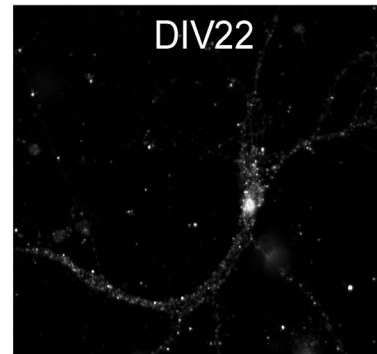
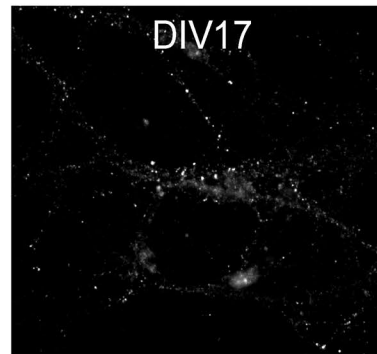
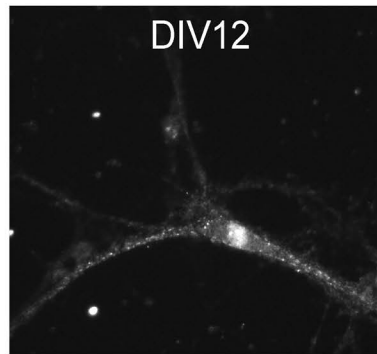
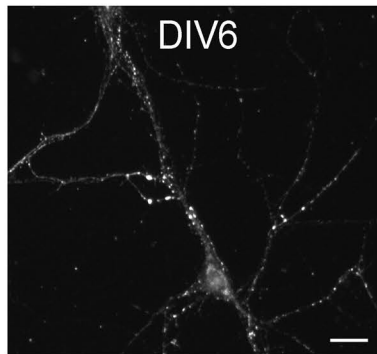
C



B

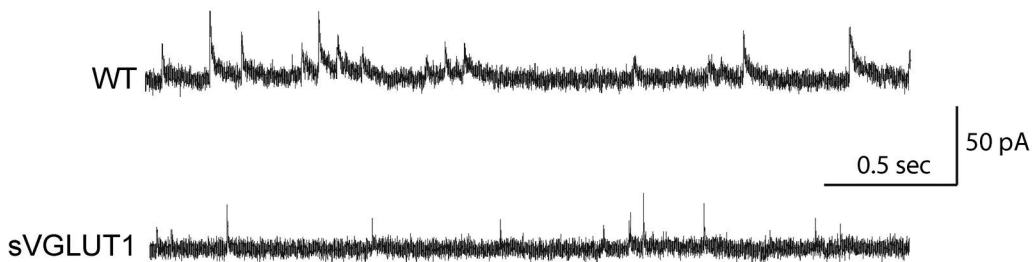
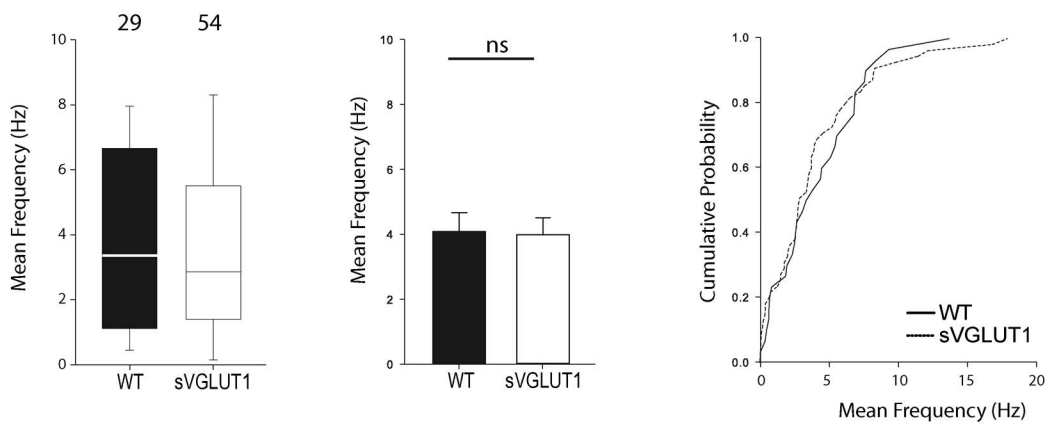
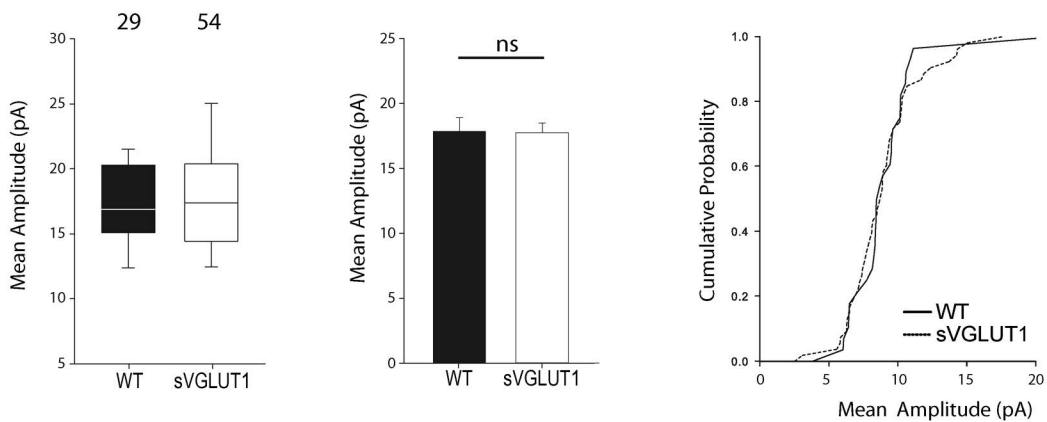


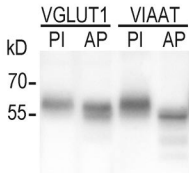
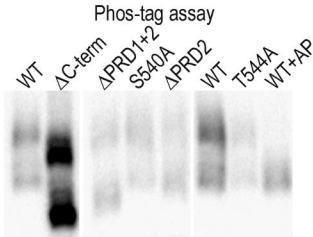
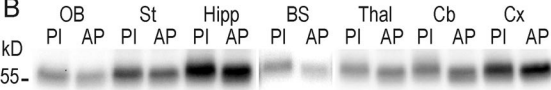


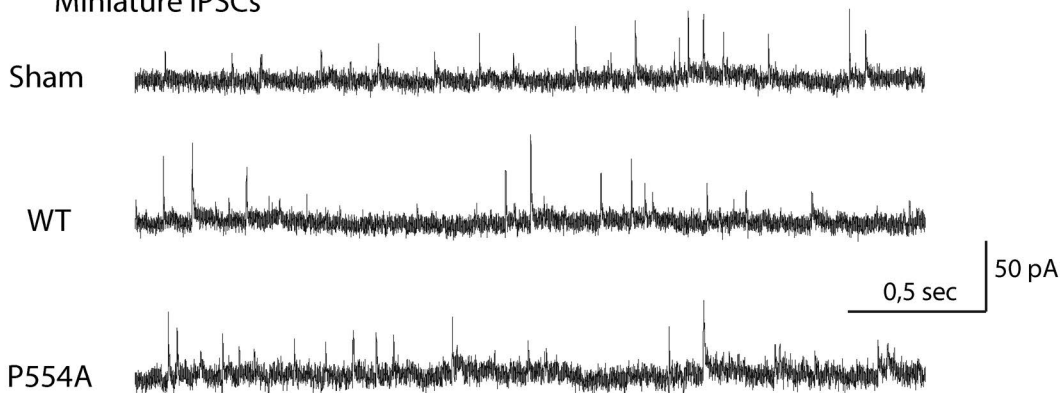
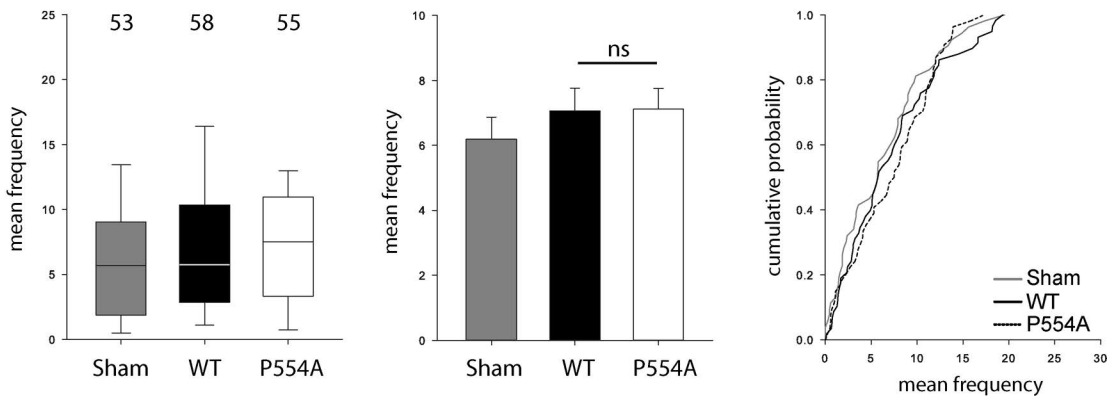
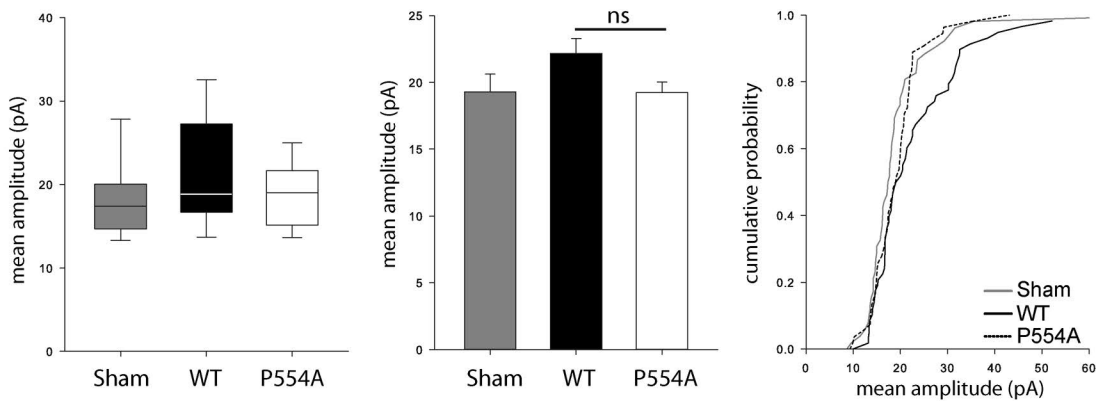


A

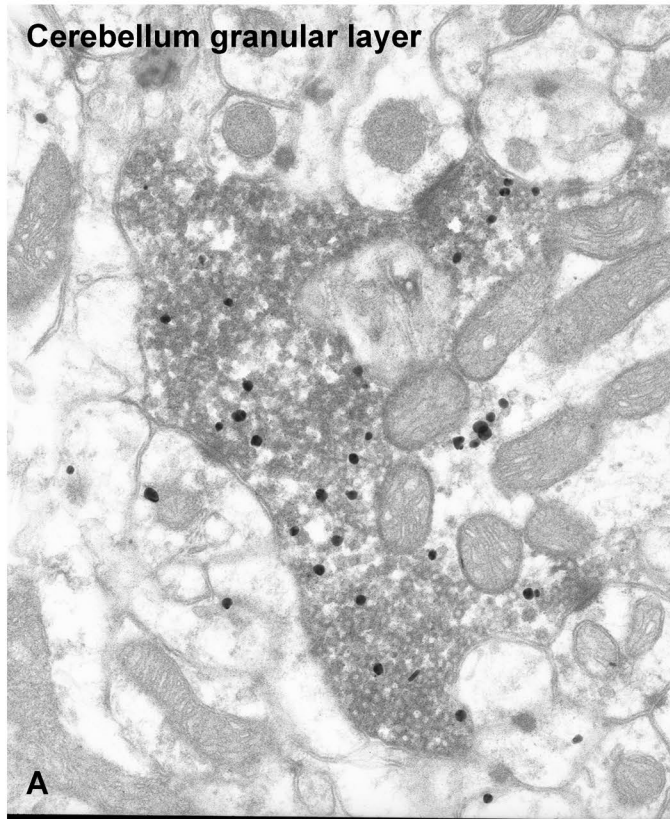
Miniature IPSCs

**B****C**

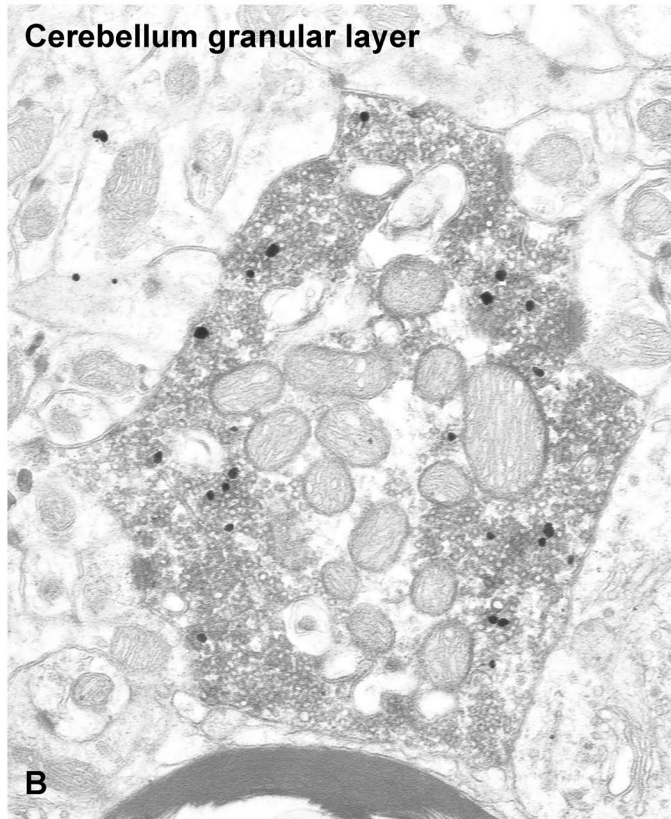
A**C****B**

A**Miniature IPSCs****B****C**

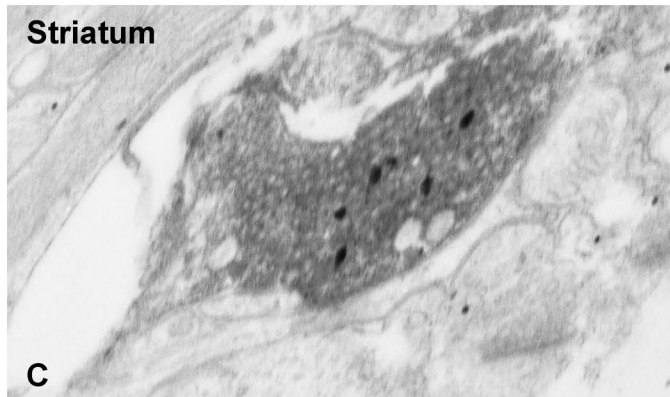
Cerebellum granular layer



Cerebellum granular layer



Striatum



Striatum

